T.C.
MANISA CELAL BAYAR UNIVERSITY
INSTITUTE OF GRADUATE EDUCATION

MASTER'S THESIS
BIOENGINEERING DEPARTMENT
BIOENGINEERING PROGRAM

2D AND 3D *IN VITRO* ALZHEIMER'S DISEASE MODEL

Dilara SABIRTAŞ

Advisor
Asst. Prof. Dr. Şeyma TAŞDEMİR

MANİSA–2025

DİLARA SABIRTAŞ

2D AND 3D *IN VITRO* ALZHEIMER'S DISEASE MODEL

2025

UNDERTAKING

I hereby declare that this thesis was written in accordance with academic and ethical rules at Manisa Celal Bayar University Graduate Education Institute Bioengineering Department and that all literature information used is included in the thesis by referencing, that it is entirely my own work, that I have cited every quotation, and that I have not used any artificial intelligence or program that is against academic and ethical rules in writing the thesis.

Signature
Dilara SABIRTAŞ

ÖZET

Yüksek Lisans Tezi

Dilara SABIRTAŞ
Manisa Celal Bayar Üniversitesi
Lisansüstü Eğitim Enstitüsü
Biyomühendislik Anabilim Dalı

Danışman: Dr. Öğretim Üyesi Şeyma TAŞDEMİR

Alzheimer hastalığı (AH) bilişsel gerileme ile tanımlanan nörodejeneratif bir hastalıktır. AH'nin en bilinen patofizyolojisi; Aβ peptitlerinin ve fosforile olmuş Tau proteininin birikimidir. Aβ peptitlerinin birikimi senil plaklar ile sonuçlanırken; fosforile olmuş Tau nörofibriler yumak oluşumuna neden olmaktadır. Diğer patofizyolojiler ise nöroinflamasyon, kolinerjik nöron dejenerasyonu ve genetik bozulmalar olarak sayılmaktadır. Dünya genelinde milyonlarca insanı etkileyen ve en yaygın görülen nörodejeneratif hastalık olan AH'nin tam olarak patogenezinin aydınlatılması, evrelerinin anlaşılması ve yeni tedavi stratejilerinin geliştirilmesi için güvenilir ve gerçeğe yakın in vitro modellere ihtiyaç duyulmaktadır. Bu tez çalışmasında, AH'ye yönelik ilaç etken madde araştırmalarına katkı sağlamak amacıyla yenilikçi in vitro modeller oluşturulması amaçlanmıştır. Bu doğrultuda, SHSY5Y ve N9 hücre hatlarının $A\beta_{1-42}$ peptidi ile birlikte, hem iki boyutlu (2B) hem de mikro doku tekniğiyle üç boyutlu (3B) in vitro AH modelleri geliştirilmiştir. Modelleme sürecinde, ilk olarak patofizyolojik bir belirteç olan Aβ peptidi kullanılarak, kolinerjik nöron özellikleri taşıyan SHSY5Y hücre hattı ile hem 2B hem de 3B in vitro modeller oluşturulmuştur. Ardından, AH'nin immün sistem ile ilişkisini incelemek ve in vivo'ya daha benzer bir model oluşturabilmek amacıyla modele mikroglia hücresi olan N9 hattı eklenmiş; mikroglial aktivasyonu sağlamak için ortama lipopolisakkarit (LPS) ilave edilmiştir. Sonrasında oluşturulan AH modellerinin karakterizasyonu için Alamar mavisi ile hücre canlılığı, gerçek zamanlı polimeraz zincir reaksiyonu (Q-PCR) ile AH ile ilişkili genlerin ekspresyon seviyesinin belirlenmesi, asetilkolin esteraz (AchE) aktivitesi ve fosforillenmiş tau (pTau) miktarı ölçümü yapılmıştır. Elde edilen bulgular sadece SHSY5Y hücreleri ile geliştirilen 3B in vitro AH modelinin gelecek araştırmalar için önemli bir umut vaat ettiğini ortaya koymaktadır. Bununla birlikte, SHSY5Y ve N9 hücrelerinin ko-kültürü ile oluşturulan, nöroinflamasyon hipotezine dayalı 2B ve 3B AH modellerinde, hücre-hücre etkileşimi ve proinflamatuar aktivite beklenen düzeyde gözlemlenememiştir. Elde edilen bu bulgu, hücreler arası etkileşimlerin modellenmesinde hücre tipi uyumunun kritik rolünü ortaya koymaktadır.

Anahtar Kelimeler: Alzheimer Hastalığı, in vitro hastalık modelleri, mikro doku, 3B kültür, mikroglia

2025, 82 sayfa

ABSTRACT

M.Sc. Thesis

Dilara SABIRTAŞ

Manisa Celal Bayar University
Graduate School of Education
Department of Bioengineering

Supervisor: Asst. Prof. Dr. Şeyma TAŞDEMİR

Alzheimer's disease (AD) is a neurodegenerative disease characterized by cognitive decline. The most well-known pathophysiology of AD is the accumulation of Aβ peptides and phosphorylated Tau protein. The accumulation of Aβ peptides results in senile plaques, while phosphorylated Tau leads to the formation of neurofibrillary tangles. Other pathophysiologies include neuroinflammation, cholinergic neuron degeneration, and genetic disorders. Reliable and realistic *in vitro* models are needed to fully elucidate the pathogenesis of AD, the most common neurodegenerative disease affecting millions of people worldwide, understand its stages, and develop new treatment strategies. This thesis aims to create innovative *in vitro* models to contribute to drug-active ingredient research for AD. In this regard, *in vitro* AD models were developed using both two-dimensional (2D) and three-dimensional (3D) micro-tissue techniques using the $A\beta_{1-42}$ peptide of SHSY5Y and N9 cell lines. During the modeling process, both 2D and 3D *in vitro* models were created using the SHSY5Y cell line, which exhibits cholinergic neuron characteristics, using the Aβ peptide, a pathophysiological marker. Subsequently, to examine the relationship between AD and the immune system and to create a model more similar to the *in vivo* model, the N9 microglial cell line was added to the model. Lipopolysaccharide (LPS) was added to the medium to ensure microglial activation. Subsequent characterization of the generated AD models included cell viability with Alamar Blue™, quantitative real-time polymerase chain reaction (qRT-PCR) to determine the expression levels of AD-related genes, acetylcholine esterase (AchE) activity and phosphorylated tau (pTau) levels. The findings suggest that the 3D *in vitro* AD model developed exclusively with SHSY5Y cells holds significant promise for future research. However, in 2D and 3D AD models based on the neuroinflammation hypothesis, created by co-culture of SHSY5Y and N9 cells, cell-cell interactions and proinflammatory activity were not observed at the expected levels. This finding demonstrates the critical role of cell type compatibility in modeling intercellular interactions.

Keywords: Alzheimer's Disease, *in vitro* disease model, microtissue, 3D culture, microglia

2025, 82 pages

PREFACE AND ACKNOWLEDGMENTS

This thesis was conducted on 2D and 3D *in vitro* models generated using SHSY5Y and N9 cell lines to better understand Alzheimer's disease. The thesis consists of five sections: introduction, materials and methods, results, discussion, conclusion, and recommendations. The unique value of this study was the creation of a more realistic Alzheimer's disease model by co-culturing SHSY5Y and N9 cells using a 3D Petri Dish method and adding amyloid beta and lipopolysaccharide to the medium. The study aimed to analyze disease-specific biomarkers, assess cytotoxicity levels, and identify changes in gene expression.

I would like to thank Health Institutes of Türkiye (TÜSEB) for supporting my project number 37541 with the program number 2023-A2-02, which made it possible to research my thesis. I also gratefully acknowledge the support of TÜBİTAK, provided under the 1001 Program with project number 122S035.

First and foremost, I would like to express my deepest gratitude and heartfelt appreciation to Assoc. Prof. Dr. Deniz KARATAŞ, who guided me with unwavering support and an inspiring approach throughout my master’s journey.

I'd like to thank all my fellow travelers, who have given me rides, sometimes chatting, sometimes staying silent, throughout my countless hitchhiking experiences, whether I remember them or not. Without them, I wouldn't have been able to reach this point in this journey.

I offer my deepest gratitude and love, especially to “Gülüm”, my one and only Zümral, and my dear friend Ali Mert who reminded me, in moments of doubt, that both falling and rising are part of this journey. I’m truly grateful to have you in my life.

I'd like to thank Assoc. Prof. Dr. Aylin ŞENDEMİR, who opened her laboratory to me and made significant contributions to my scientific work, and the entire EBIOPHASE team, especially Dr. Pelin ÇORUK İLHAN and Ali İLHAN, for showing me that we can be a family in academia. I'd also like to express my gratitude to Cenk Çelik, a former EBIOPHASE member, for his invaluable assistance in designing the graphical abstract.

I would like to thank Prof. Dr. Sinem Ezgi TURUNÇ ÖZOĞLU from Katip Çelebi University Faculty of Pharmacy for the qRT-PCR analyses.

I would like to wholeheartedly thank my dear friends Zehra Gül MORÇİMEN, Umut Doğu SEÇKİN and Merve BAŞOL, who made me feel that they were with me during my master's degree and illuminated my path with their knowledge and support.

I would like to thank my dear aunt Zeynep ÇAKMAK and my uncle İsmail ÇAKMAK for opening their home to me and providing a warm and peaceful environment throughout this process. I am deeply grateful to my big family who has always stood by my side; to my beloved mother, father, and little brother; and above

all, to my family who supported the little Dilara within me and allowed the young scientist inside her to grow throughout this journey.

Finally, I would like to express my sincere gratitude to my academic advisor, Dr. Şeyma TAŞDEMİR, for creating a safe and supportive space for me both academically and personally. Her ability to challenge me when needed, to listen with empathy, and to stand by me with support has been invaluable. I have been fortunate to share the joy of scientific discovery with her, and I deeply admire her visionary guidance. It is truly an honor to be her student.

Dilara SABIRTAŞ
Manisa, 2025

INDEX OF SYMBOLS AND ABBREVIATIONS

Aβ	Amyloid-β
AChE	Acetylcholinesterase
AD	Alzheimer's Disease
APOE	Apolipoprotein E
APP	Amyloid Procursor Protein
β-Act	Beta Actin
BBB	Blood Brain Barrier
BDNF	Brain Derived Neurotrophic Factor
cDNA	complementary Deoxyribose Nucleic Acid
ChAT	Choline Acetyltransferase
CNS	Central Nervous System
CREB	Cyclic Adenosine Monophosphate Response Element Binding Protein
DMEM HG	Dulbecco's Modified Eagle Medium, High Glucose
DMSO	Dimethyl Sulfoxide
DNA	Deoxyribose Nucleic Acid
EOAD	Early Onset Alzheimer's Disease
FBS	Fetal Bovine Serum
hIPSCs	Human Induced Pluripotent Stem Cells
IL	Interleukin
LOAD	Late Onset Alzhimer's Disease
LPS	Lipopolysaccharide
MAP	Microtubule Associated Protein
mRNA	messenger Ribonucleic Acid
MTT	3-(4,5-Dimetiltiyazol-2-yl)-2,5-Diphenyltetrazolium Bromide
NP	Neurofibrillary Tangle
PBS	Phosphate Buffer Solution
PCR	Polymerase Chain Reaction
RNA	Ribonucleic Acid
SP	Senile Plaque
T2DM	Type 2 *diabetes mellitus*
Tm	Melting Temperature

INDEX OF FIGURES

Page

Figure 1: Schematic representation of LOAD and risk factors causing LOAD (Valdez-Gaxiola et al., 2024) 2
Figure 2: Tau protein status in healthy and AD patients (Krishnamurthy et al., 2025) 7
Figure 3: AchE formation and its consequences (Gajendra et al., 2024) 8
Figure 4: Schematic representation of experimental design 15
Figure 5: 2D Alzheimer's Disease Model Experimental Images at different $A\beta_{1-42}$ concentrations and on different days (4X magnification, Olympus CK40) 29
Figure 6: 3D Alzheimer's Disease Model Experimental Images at different $A\beta_{1-42}$ concentrations and on different days (10X magnification, Olympus CK40) 32
Figure 7: Growth Kinetics Results of N9 Cells in RPMI Medium 33
Figure 8: Growth Kinetics Result of N9 Cells in DMEM HG Medium 34
Figure 9: Coculture Results of SHSY5Y and N9 Cells 34
Figure 10: Experimental Images of 2D Coculture Alzheimer's Disease Model at Different $A\beta_{1-42}$ Concentrations and Different Days (4X magnification, Olympus CK40) 37
Figure 11: Experimental Images of 3D Coculture Alzheimer's Disease Model at Different $A\beta_{1-42}$ Concentrations and Different Days (10X magnification, Olympus CK40) 39
Figure 12: Cell viability data after 24 hours of incubation to determine the optimum $A\beta_{1-42}$ peptide concentration in a 2D AD model 40
Figure 13 : Cell viability data after 48 hours of incubation to determine the optimum $A\beta_{1-42}$ peptide concentration in a 2D AD model 41
Figure 14: Cell viability data after 72 hours of incubation to determine the optimum $A\beta_{1-42}$ peptide concentration in a 2D AD model 41
Figure 15: Cell viability data after 24-hour incubation to determine the optimum $A\beta_{1-42}$ peptide concentration in a 3D monoculture AD model 42
Figure 16: Cell viability data after 48 hours of incubation to determine the optimum $A\beta_{1-42}$ peptide concentration in a 3D AD model 42
Figure 17: Cell viability data after 48 hours of incubation to determine the optimal $A\beta_{1-42}$ peptide concentration in the 2D Co-culture AAD model 43
Figure 18: Cell viability data after 48 hours of incubation with 1 mg/mL LPS to determine the optimal $A\beta_{1-42}$ peptide concentration in the 3D Co-culture AD model 43
Figure 19: Relative APP, ADAM9, BACE1, MAPT, ACHE, BDNF and CREB genes expression levels in 2D model groups 45
Figure 20: Relative APP, ADAM9, BACE1, MAPT, ACHE, BDNF and CREB expression levels of 3D AD and Control groups 46
Figure 21: Relative APP, ADAM9, BACE1, MAPT, ACHE, BDNF and CREB expression levels of 2D co-culture AD and control groups 47

Figure 22: Relative APP, ADAM9, BACE1, MAPT, ACHE, BDNF and CREB expression levels of 3D co-culture AD and control groups 49
Figure 23: Standard curve used for BCA analysis 49
Table 5: Protein values measured in the AD model and control group 50
Figure 24: Standard Curve Used for Determination of AchE Activity 51
Figure 25: AchE Analysis in 2D AD Model 51
Figure 26: AchE Analysis in 3D AD Model 52
Figure 27: AchE Analysis in 2D Coculture AD Model 52
Figure 28: AchE Analysis in 3D Coculture AD Model 53
Figure 29. Standard curve graph created to calculate human pMAPT/pTAU amount 54
Figure 30: pMAP/TAU Analysis in 2D AD Model 54
Figure 31: pMAP/TAU Analysis in 3D AD Model 55
Figure 32: pMAPT/pTAU Analysis in 2D Co-Culture AD Model 55
Figure 33: pMAPT/pTAU Analysis in 3D Coculture AD Model 56

TABLE INDEXES

Page

Table 1: Concentrations and purities of RNAs obtained from control and 2D AH model groups 44
Table 2: Amount and purity of RNA obtained from the 3D AD model and control group 45
Table 3: Amount and purity of RNA obtained from the 2D co-culture AD model and control group 47
Table 4: Amount and purity of RNA obtained from the 3D co-culture AD model and control group 48
Table 5: Protein values measured in the AD model and control group 50

CONTENT

ÖZET i
ABSTRACT ii
INDEX OF SYMBOLS AND ABBREVIATIONS v
INDEX OF FIGURES vi
TABLE INDEXES viii
CONTENT ix
SECTION ONE 1
1. INTRODUCTION 1
1.1 Alzheimer's Disease Types 1
1.1.1 Early Alzheimer's Disease 2
1.1.2 Late Alzheimer's Disease 3
1.2 Alzheimer's Disease Pathological Markers 6
1.3 Engineered Models of Disease 8
1.3.1 2 Dimensional (2D) Disease Models 8
1.3.2 3 Dimensional (3D) Disease Models 9
1.4 *In vitro* Alzheimer's Disease Models 11
1.5 Neuroinflammation Associated with Alzheimer's Disease 12
SECTION TWO 15
2.MATERIALS & METHODS 15
2.1 Study Design 15
2.1. Cultivation, Passaging and Stocking of SHSY5Y and N9 Cells 16
2.2 Engineered Model of AD Disease 17
2.2.1 Preparation of $A\beta_{1-42}$ Peptide Stock 17
2.2.2 Development of 2D AD Model 17
2.2.3 Development of 3D AD Model 18
2.2.4 2D *in vitro* Co-Culture AD Model 18
2.2.4.3 Development of a 2D *in vitro* Co-Culture AD Model 20
2.3 Characterization of AD Model 21
2.3.1 Alamar Blue™ Assay 21
2.3.2 Quantitative Real Time Polymerase Chain Reaction (qRT-PCR) 22
2.3.3 Bicinchoninic Acid (BCA) Assay 24
2.3.5 pMAPT/pTau Amount Determination 25
2.3.6 Acethylcholinesterase (AchE) Activity Assay 26
SECTION THREE 28

3. RESULTS 28
3.1 Alzheimer's Disease Model 28
3.1.1 2D Alzheimer's Disease Model 28
3.1.2 3D Alzheimer's Disease Model 29
3.1.3 Co-culture 2D Alzheimer's Disease Model 32
3.1.3.3 Growth Kinetics of N9 Cells in DMEM HG Medium 33
3.1.4 Co-culture 3D Alzheimer's Disease Model 37
3.2 Cell Viability 40
3.2.1 2D Cell Viability 40
3.2.2 3D Cell Viability 41
3.2.3 2D Co-Culture Cell Viability 42
3.2.4 3D Co-Culture Cell Viability 43
3.3 Quantitative Real Time Polymerase Chain Reaction (qRT-PCR) 44
3.3.1 qRT-PCR Results for 2D AD Model 44
3.3.2 qRT-PCR Results for 3D AD Model 45
3.3.3 qRT-PCR Results for 2D Co-Culture AD Model 46
3.3.4 qRT-PCR Results for 3D Co-Culture AD Model 48
3.4 Bicinchoninic Acid Assay (BCA) 49
3.5 Acetylcholinesterase (AchE) Activity 50
3.5.1 AchE Activity in 2D AD Model 51
3.5.2 AchE Activity in 3D AD Model 52
3.5.3 AchE Activity in 2D Co-Culture AD Model 52
3.5.4 AchE Activity in 3D Co-Culture AD Model 53
3.6 pMAPT/pTau Assay 53
3.6.1 pMAPT/pTAU Analysis in 2D AD Model 54
3.6.2 pMAPT/pTAU Analysis in 3D AD Model 55
3.6.3 pMAPT/pTAU Analysis in 2D Co-Culture Model 55
3.6.4 pMAPT/pTAU Analysis in 3D Co-Culture Model 56
SECTION FOUR 57
4. DISCUSSION 57
SECTION FIVE 63
5. CONCLUSION & RECOMMENDATIONS 63
5. REFERENCES 65

SECTION ONE

1. INTRODUCTION

Alzheimer's Disease (AD) was first discovered by German Alois Alzheimer, who give name to disease in 1907. After pathological examination of the brain of a 51-year-old woman showing signs of dementia, Alois Alzheimer discovered neurofibrillary tangles (NFT) and senile plaques (SP) in the cerebral cortex of the brain (Ramirez-Bermudez, 2012).

AD is an advanced stage of dementia that includes various behavioral disorders, memory impairments, and cognitive decline (Jack et al., 2018). In addition, dementia in AD has been reported to occur before the disease is diagnosed. According to data published in 2024, there are 35 million people with AD. A quarter of a century later, it is estimated that 140 million people suffering from AD (Abdul Manap et al., 2024).

In the early stages of AD, individuals may experience attention deficits and difficulty concentrating. This is due to a disorder in the temporal periphery of the brain (Farooq et al., 2022). In the advanced stages of Alzheimer’s disease, symptoms may manifest through both psychological and behavioral alterations. Alterations can significantly impact the quality of life of both the patient and their caregiver. These symptoms can also affect the individual's mood, such as hallucinations, depression, anxiety, and aggression (Cerejeira et al., 2012; Farrimond et al., 2012).

1.1 Alzheimer's Disease Types

When diagnosing AD, the age of the patient at diagnosis is crucial. AD is examined in two ways: Early Onset AD (EOAD) which patients are known to be younger than 65 age and Late Onset AD (LOAD) which patients are known to be older than 65 age. This is because the causes of EOAD and LOAD are different. Approximately 5% of AD patients are reported as EOAD cases, and almost all cases are reported as early-onset Alzheimer's due to genetic factors (Udin et al., 2021).

95% of people with AD are diagnosed with LOAD. The occurrence of LOAD in an individual depends on factors such as genetic factors, environment and lifestyle, hypertension, epidemiological factors, metabolic derangement, and neuroinflammation. A schematic representation of the types and causes of Alzheimer's disease is shown in Figure 1 (Wightman et al., 2020; Chaudhary et al., 2018; Stoccoro et al., 2017; Eskandari-Sedighi and Blurton-Jones, 2023; Raulin et al., 2019).

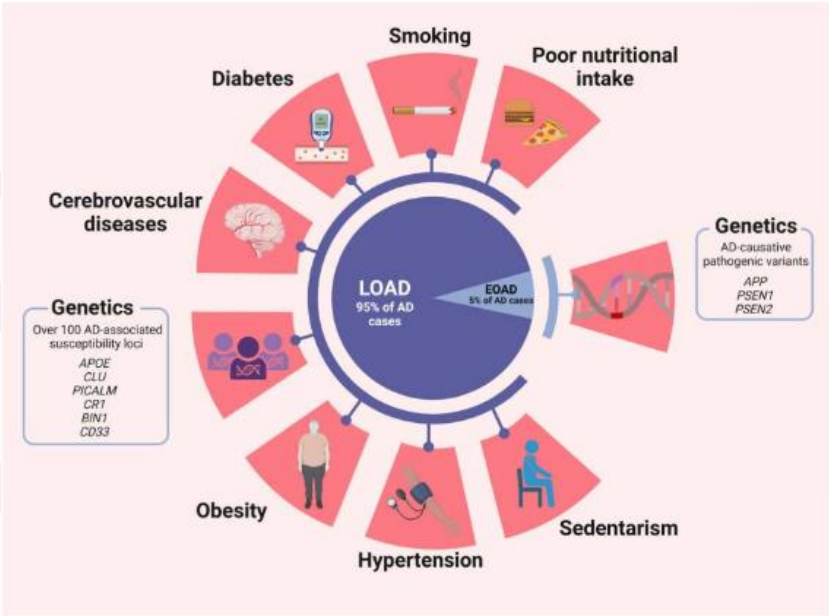

Figure 1: Schematic representation of LOAD and risk factors causing LOAD (Valdez-Gaxiola et al., 2024)

A detailed review of the risk factors for EOAD and LOAD is provided below.

1.1.1 Early Alzheimer's Disease

Three genes are responsible for the development of EOAD: Amyoid Precursor Protein (*APP*) gene which encodes APP, Presenilin 1 (*PSEN1*), and Presenilin 2 (*PSEN2*) (Dai et al., 2017). They are located on chromosomes 21, 14, and 1, respectively (Levy et al., 1995).

When evaluated for EOAD, the most common mutation in the disease is found in the *PSEN1* gene. Mutations in the *PSEN1* and *PSEN2* genes lead to increased

encoding of the γ-secretase enzyme complex, which cleaves the membrane of the APP protein (Sherrington et al., 1995). Patients diagnosed with EOAD have autosomal dominant *PSEN1* and *PSEN2* mutations, which are transmitted to the next generation (Reitz et al., 2011).

The APP gene produces the integral membrane protein APP. This protein is responsible for synaptic protection and synaptic flexibility (Priller et al., 2006). APP is proteolyzed by β-secretase to form the β peptide, and α-secretase to form the α peptide (Bird, 2008). If this occurs, mutations in the *APP* gene are responsible for 10–15% of the cases of EOAD, and 69 missense mutations have been reported (Scheuner et al., 1996).

1.1.2 Late Alzheimer's Disease

Unlike EOAD, LOAD has multiple causes, including genetic factors, environmental influences (heart diseases, dietary habits, addictions, physical activity), and pathological characteristics (Wightman et al., 2020).

The gene responsible for LOAD is the apolipoprotein E (*APOE)* gene. Mutations in the *APOE* genes alleles, which *APOE4* alleles can cause damage or increase amyloid-β (Aβ) accumulation in the medial temporal lobe of the brain, which is responsible for memory and learning (M Di Battista et al., 2016). The *APOE4* allele has been found to increase the severity of pathological findings associated with the disease, not only in AD but also in other types of neurodegenerative diseases such as Parkinson's (Pankratz, N et al., 2006).

The APOE protein is found in two distinct regions: the periphery and the central nervous system (CNS). The reason for this different location is the blood-brain barrier (BBB) (Linton et al., 1991). While peripheric APOE and CNS-based APOE cause AD, their pathogenesis differs due to their locations and functions. Peripheral APOE is important for cardiovascular health and immune regulation (Liu et al., 2013). CNS-based APOE is responsible for lipid and cholesterol transport for the formation of new synapses and repair of newly formed tissues (Bu, 2009). Conversely, CNS-based APOE is overexpressed, in the presence of activated microglia or pathological markers that appear in the presence of neurodegenerative disease (Raulin et al., 2022).

Another important factor that plays a role in Alzheimer's disease is thought to be the immune system, namely microglia, found in the central nervous system. Microglia are innate cells that protect the brain from factors such as viruses, bacteria, cell debris, and trauma (Perdiguero et al., 2015). In addition to pathological conditions, they are also responsible for cell homeostasis. They also have various functions, such as regulating myelination and neuronal plasticity (Long et al., 2022). In fact, they also play an active role in EOAH and LOAH (Sudduth et al., 2013). However, while gene mutations are generally responsible for EOAH, it is thought that microglia, due to their overactivation, may cause LOAH (Salih et al., 2019; Zhouet al., 2018).

Because NFTs originating from Aβ plaques in EOAH eliminate cells that should undergo apoptosis through phagocytosis, thus providing a healthy transition from the proinflammatory M1 phase to the anti-inflammatory M2 phase, thus showing protective properties (Hickman, et al., 2008).

However, the situation is more complicated in LOAH. Because microglia are overactivated in LOAH, the proinflammatory phase lasts longer than expected. A prolonged proinflammatory phase means increased neurotoxicity. This occurs through the release of cytokines such as tumour necrosis factor-α (TNF-α), interleukin-6 (IL-6), IL-1β, and IL-12 over a longer period of time (Colonna and Butovsky, 2017). While microglia clear Aβ peptide and phosphorylated tau (pTau) proteins, which are pathological hallmarks of AD, they also release cytokines such as TNF-α and IL-1β, causing both cognitive loss due to neuronal damage and the progression of AD (Ismail et al., 2020). On the other hand, overactivated microglia trigger the formation of ptau protein, causing synapse apoptosis. In short, this causes an endless cycle between the long M1 phase and the short M2 phase, thus exacerbating AD (Hansen et al., 2018).

Another immune response associated with AD is the adaptive immune system, and astrocytes are responsible for this. Astrocytes are also located in the CNS (Sun and Jakobs, 2012). Astrocytes are responsible to regulating ion balance, they contribute to BBB integrity and are also responsible for homeostasis in the brain. Astrocytes activated by brain damage such as pathogens or trauma (Dai et al., 2023). However, in the brain with a disrupted BBB, in a neurotoxic environment, they can release signals to attract white blood cells or peripheral macrophages present in the body to the cerebral parenchyma, the part of the brain where neurons and glia receive support (Price et al., 2021).

Similar to microglia, A1 and A2 phases are observed. The A1 phase is responsible for pro-inflammation, while the A2 phase is responsible for anti-inflammation. Aβ or neurofibrillary tangles (NFTs) accumulation leads to a change in astrocyte morphology. In advanced AD, as in microglia, they can cause neuronal damage. This neuronal damage results in an increase in NFT levels (Stanca et al., 2023).

Another cause of late-onset Alzheimer's disease is sedentarism (Gogniat et al., 2025). Sedentarism or inadequate exercise can trigger physiological changes in the brain that can lead to neuroinflammation. *in vitro* and *in vivo* studies suggest that being physically active and exercising regularly increases microglial homeostasis (Diniz et al.,2024). They also revealed that people who exercise regularly have higher levels of presynaptic proteins, which facilitate neural connections in the brain (Casaletto et al., 2022).

Type 2 *diabetes mellitus* (T2DM) is the inability of cells to respond to the insulin hormone, resulting in insufficient insulin production and hyperglycemia which is LOAD and T2DM are closely linked (Duran et al., 2022). Insulin resistance leads to Aβ accumulation in the brain, leading to senile plaque formation (Hayden, 2019). Furthermore, insulin resistance triggers apoptosis in neurons, initiating inflammation, and thus contributing to the pathogenesis of AD and the progression of dementia (Wainaina et al., 2014).

Another cause of late-onset Alzheimer's disease is smoking. Smoking increases reactive oxygen species in the brain, leading to Aβ accumulation and synaptic dysfunction. Because reactive oxygen species are highly reactive. Normally they regulate the cellular signalling pathways and homeostasis. Their overexpression in the brain causes neurodegenerative diseases markers (Wang et al., 2014). Smoking also disrupts the regulation of the APP protein, leading to the formation of pTau. Smoking also contributes to vascular dementia in the brain, causing an imbalance in cerebral blood flow. Smoking also causes inflammation in the brain. It triggers the immune system, leading to overactivation of microglia (Honda et al., 2004).

Cardiovascular disease and LOAD cause cognitive decline, their relationship has recently become a focus of research. This is primarily because both diseases share common risk factors such as smoking, hypertension, poor nutritional intake, obesity

and insulin resistance (Nordestgaard et al., 2022). Another contributing factor is inflammation, as chronic inflammation and oxidative stress occur in individuals with cardiovascular disease. This process, as mentioned above, can ultimately lead to brain degeneration and the emergence of AD pathological markers (Gong et al., 2021).

Genes expressed at the cellular level are also responsible for AD. These genes include *APP, ADAM9, BACE1, MAPT, ACHE*, Brain-Derived Neurotrophic Factor (*BDNF*) and *CREB*. These genes expressions are just a few of the genes known to cause AD. Cleavage of APP produced from the *APP* gene by β-secretase and γ-secretase leads to Aβ accumulation. This accumulation results in the formation of senile plaques, which cause neurotoxicity (Mórotz et al., 2019). Downregulation of *ADAM9* gene expression also leads to cleavage of APP by α-secretase, leading to Aβ accumulation. *BACE1* is the gene responsible to produce β-secretase, and its overexpression also results in the pathological hallmark of AD (Chen et al., 2012). The *MAPT* gene is responsible for tau protein synthesis. *ACHE* is responsible for the acetylcholine esterase protein and has been reported to be increased in AD (Wang et al., 2009). The *BDNF* gene encodes a protein responsible for neuronal development and plasticity. A decrease in the *BDNF* gene is observed in AD (Caccamo et al., 2010). *CREB* is responsible for the transcription factor that regulates the expression of genes like *BDNF* in the brain (Jin et al., 2013).

1.2 Alzheimer's Disease Pathological Markers

Mutations in the APP gene lead to the formation of the most toxic form of the Aβ peptide, the pathological marker in AD. This form accumulates and causes the formation of Aβ plaques (Yan and Wang, 2006). This specific histopathological finding that is checked for in the diagnosis of AD. These include the accumulation of Aβ, the formation of NFTs by pTau, and the decrease or degeneration of cholinergic neurons (Murphy and LeVine, 2010; Stanciu et al., 2020).

Tau protein normally functions to stabilize neuronal microtubules. However, hyperphosphorylated tau protein accumulates in the brain, forming neurofibrillary tangles and contributing to the development of AD (Stanciu et al., 2020). Tau is microtubule associated protein, which binds to microtubules in neurons responsible for axonal transport (Weingarten et al., 1975). In the healthy brain, tau protein

phosphorylation is important for maintaining the structural integrity of microtubules. However, when it becomes hyperphosphorylated, it disrupts the structural integrity of axons and leads to the formation of NFTs in the neocortex (Jicha et al., 1997). Below is a schematic representation of what tau protein looks like in healthy individuals and those with AD. While tau found in healthy axonal regions is found in a soluble form, it is found in three different forms in the axons of individuals suffering from AD: soluble, fibrillated, and oligomeric (Krishnamurthy et al., 2025).

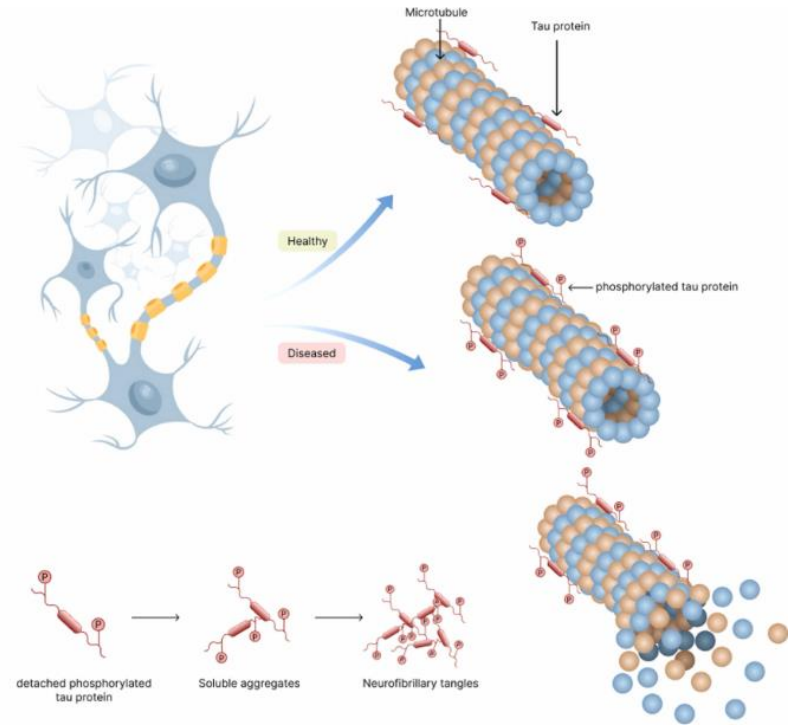

Figure 2: Tau protein status in healthy and AD patients (Krishnamurthy et al., 2025)

Acetylcholine (ACh), a neurotransmitter secreted by cholinergic neurons, is responsible for memory and learning. Damage to these neuron types reduces the amount of ACh secreted, aided by the enzyme acetylcholine esterase (AChE). This, in turn, may contribute to the development of AD by causing the production of Aβ peptide and hyperphosphorylation of tau (Chen et al., 2022). AchE formation and its consequences are shown in Figure 3.

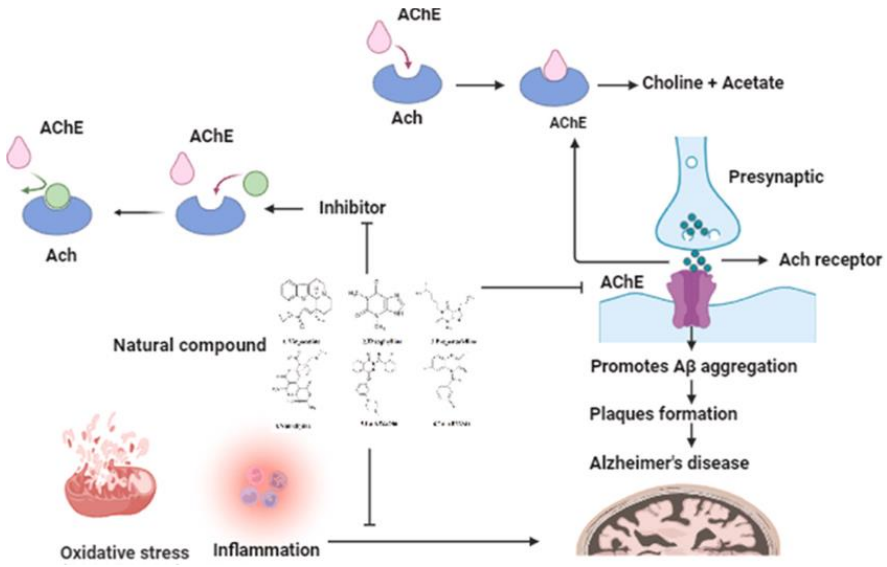

Figure 3: AchE formation and its consequences (Gajendra et al., 2024)

1.3 Engineered Models of Disease

The goal of many disease modeling studies is to understand disease mechanisms or develop new treatments. Although progress has been made in *in vivo* disease modelling, the targeted disease model remains elusive due to physiological and structural differences between species (Phan et al., 2017). These limitations can lead to therapeutic drugs with confirmed preclinical efficacy failing in the clinic or to a lack of complete understanding of the disease mechanism. To overcome these limitations, new *in vitro* disease models, including different cell types and building block molecules, need to be developed (Benam et al., 2015). *In vitro* disease models are divided into two main groups: 2D and 3D models.

1.3.1 2 Dimensional (2D) Disease Models

2D *in vitro* models are models in which cells are grown in a single layer in a petri dish or flask. *In vitro* 2D models offer the advantage of being easier to perform, faster, and more cost-effective than *in vivo* models (Fogliette et al., 2021). Despite these advantages of 2D *in vitro* models, there are limitations such as distortion in cell morphology and therefore not being able to fully reflect the function and mechanism of the disease or tissue being modeled and not being able to adequately mimic tissue

complexity (Kapałczyńska et al., 2016). Another limitation of 2D models is that cell surface receptors grown in a single layer are exposed to more therapeutic agents than those in a 3D environment. This causes cells to respond differently to toxicological studies conducted on them than those in the organism (Louit et al., 2023).

As an alternative to traditional 2D *in vitro* models, human induced pluripotent stem cells (hIPSCs) are also being used. Their superiority over traditional methods includes their ability to differentiate into the desired cell type. Because they are derived from individual somatic cells, they also carry the patient's genetic background, making them attractive for disease modeling. In this way, personalized 2D *in vitro* disease models can be made (Liu et al., 2018). However, as a disadvantage of hIPSCs, the cell-cell and cell-matrix interaction is insufficient, which can lead to cell morphology loss, maturation and differentiation problems (Castellanos-Montiel et al., 2023).

1.3.2 3 Dimensional (3D) Disease Models

Due to the limitations of 2D *in vitro* models, studies on designing 3D diseases, tissues or organs *in vitro* that are more similar to their natural environment have accelerated (Huskin et al., 2023). Ideal 3D models are those that allow cell-cell and cell-matrix interactions, where different cell types can exist in the same environment, where sufficient nutrients and oxygen are provided, and where the physiological or pathophysiological characteristics of the tissue or disease are present (Langhans, 2018). 3D models offer the advantage of being tissue- or disease-specific, allowing for increased cell density and cell-to-cell and cell-to-matrix signals. However, they are also disadvantaged by the difficulty of standardization and the short lifespan of the models produced (Collins et al., 2019).

Animal models provide the best physiological conditions for preclinical studies and are still considered the most suitable. However, they are time-consuming and costly, and they also face numerous ethical limitations. This has led to a shift toward working with *in vitro* or *ex vivo* models (Humpel, 2015). Furthermore, due to genetic, biochemical, and metabolic differences between species, they cannot fully reflect human organisms. Therefore, *in vitro* cell culture studies are crucial for mimicking the

in vivo environment to examine the true functions and pathophysiology of tissues (Huh et al., 2011).

Conventional 2D cell culture techniques fail to capture the complex structure and physiology required for modeling the human central nervous system (CNS) and neurodegenerative diseases. Hierarchical 3D models, incorporating 3D extracellular matrix structures and cellular components, using tissue engineering methods are needed for *in vitro* simulation of neural physiology. 3D *in vitro* cultures are particularly important in disease models and drug trials because they reproduce the physiological microenvironment and can biomimetically simulate *in vivo* responses (Caleb vd. 2020). 2D cell culture studies differ in cell morphology, receptor expression, extracellular matrix communication, and overall cellular mechanisms compared to 3D cultures (Zuliani et al., 2025).

The inability to reflect the real extracellular matrix with 2D cultures leads researchers to develop alternative 3D disease models that can mimic a more realistic environment and bridge the gap between *in vitro* and *in vivo* models (Franco and Cedazo-Minguez, 2014).

In tissue engineering and regenerative medicine applications, 3D tissue modeling techniques are divided into two categories: scaffold-based and scaffold-free. In scaffold-based 3D models, the scaffolds are fabricated using polymeric or biomaterials. In scaffold-free models, cells self-assemble to form 3D structures. Cell sheeting, single-cell injection, and microtissue generation techniques are some of the techniques used to create 3D cell aggregate, spheroids and organoids models without scaffolding (Kelm and Fussenegger, 2010). 3D printing is a production technology that enables objects with desired properties and geometric shapes to be obtained by depositing successive layers on a platform (Al-Dulimi et al., 2021). With the 3D bioprinting method, the natural structures of cells are imitated and cell-cell interaction is allowed between cells. The most important factor for the models created by this method is the bioink used. Bioink contains essential materials and cells required while forming the tissue. Depending on the polymer type in the bioink, problems may occur in vascularization, oxygen distribution capacity and nutrient uptake rate (Agarwal et al.,2020). With this technology, 3D *in vitro* culture environments can be created by combining bioinks, hydrogels, cells and growth factors in appropriate shapes.

(Jammalamadaka et al., 2018). On the other hand, spheroids are an example of a scaffold-free method. Spheroids are simple 3D *in vitro* structures that mimic the natural environment of cells (Dousti et al., 2024). They can be produced using the hanging drop or 3D Petri Dish® method (Misun et al., 2020; Roopesh et al., 2022). They provide a productive microenvironment that can be used in various fields, from different cell types and cancer to drug testing (Benmeridja et al., 2020). However, large spheroids can have difficulties with heat and mass transfer, leading to necrosis of cell nuclei. Therefore, they should be optimized for the field of study (Janjić et al., 2021).

1.4 *In vitro* Alzheimer's Disease Models

The scarcity of *in vitro* models suitable for studying the human nervous system compared to *in vivo* models is a significant limitation for neuroscience research, including AD studies. Therefore, developing realistic 3D *in vitro* models is crucial. Choosing the correct cell type for simulating brain tissue in 2D and 3D models is crucial for the model. Immortalized cell lines are generally preferred for *in vitro* engineered disease models. Because primary cells which are obtained directly from tissue have limited proliferation capacity. The most commonly used cell lines are SHSY5Y, Neuro2a, PC12, MN9D, and N27 (Tarricone et al., 2022). SHSY5Y cells are widely used in AD models. This is primarily due to their sensitivity to the toxic effects of Aβ and also shows cholinergic neuron behaviour withouth differantiation. In the presence of Aβ, they can exhibit oxidative stress responses and synaptic and mitochondrial dysfunction (Stockburger et al., 2014; Dodurga et al., 2019). Their ability to differentiate into neuron-like cells, both physiologically and morphologically, is a reason they are frequently included in research compared to other cells. They are also preferred for active ingredient testing and high-throughput screening in the pharmaceutical industry. This is because they are a cell line in which mitochondrial functions can be evaluated in the presence of Aβ and they allow the changes caused by Aβ to be monitored at the cellular level (Forster et al., 2016).

Cholinergic neurons have become a focus of interest in *in vitro* AD modeling. Cholinergic neurons are associated with memory and attention. They also secrete acetylcholine, and cholinergic neurons are the first to be damaged in the development

of AD (Zhu et al., 2017). In *in vitro* AD modeling, SHSY5Y cells are incubated with retinoic acid or BDNF to induce their differentiation into cholinergic neurons (Medeiros et al., 2019). SHSY5Y cells, which differentiate into cholinergic neurons with BDNF or retinoic acid and form neurites, can exhibit cholinergic properties even without differentiation. However, undifferentiated SHSY5Y cells have been reported to have lower neuron-specific biomarkers (Dodurga et al., 2019).

3D experimental models are needed to understand AD metabolism and to develop alternative, more realistic, and effective treatment methods that can address the many variations seen in AD (Murphy et al., 2017). There are several key reasons which 3D approach is important in the AD model. Creating a degenerative environment to mimic brain structure in the AD model is a crucial step. Cell-to-cell interaction is better in 3D models than in 2D models, resulting in improved intercellular communication (Seidel et al., 2012). Neuronal differentiation occurs more rapidly than in 2D models. Senile plaques, which form due to Aβ aggregation in spheroid structures, are better formed in 3D (Raja et al., 2016). This allows for a triculture system where microglia, neurons, or astrocytes coexist. This triculture system may not occur in 2D structures and, naturally, does not fully reflect the AD mechanism (Park et al., 2018). Agholme et al. (2010) investigated the effect of 3D culture of SHSY5Y cells in extracellular matrix (ECM) gel combined with various factors reported to have neurodifferentiating effects to obtain cells with neuronal differentiation and function. The researchers demonstrated that SHSY5Y cells in the 3D gel had branched neurites, distinct neuronal morphology, expressed various neurospecific markers, and expressed mature Tau isoforms. In another study, SHSY5Y cells were cultivated on bacterial nanocellulose as a new 3D *in vitro* model that could mimic the complexity of nervous tissue (Innala et al., 2014).

1.5 Neuroinflammation Associated with Alzheimer's Disease

Microglia are the primary and innate immune cells in the central nervous system. They maintain homeostasis in the brain by initiating a proinflammatory response in the presence of pathogenic activity in the brain or in conditions such as

brain injury (Pal et al., 2022). In the AD, accumulating Aβ in the brain activates microglia, initiating a proinflammatory process as a neuroprotective response (Mathys et al., 2017). While the primary purpose of this response is to protect the brain against degeneration, the ongoing chronic inflammation caused by the presence of Aβ in individuals with AD. In people suffering from this disease microglia which can cause the initially protective effect to brain to evolve into a degenerative response over time through cytokine release (Çınar, 2022). There are also studies indicating that microglia gather around Aβ plaque and pTau protein (Heneka et al., 2024). Another feature of microglia is that they can bind to oligomers and fibrils, which are different forms of Aβ, through toll-like receptors and initiate an immune response (Heneka et al., 2015). Numerous studies in the literature examine the relationship between Aβ presence and microglial activity. For example, in a study conducted by Lin et al., (2022), it was reported that phagocytosis was observed in the study in which microglial activation was triggered with Aβ by human microglia HCM3 and human monocyte THP-1. Not only the presence of Aβ but also molecules found in the outer membrane of gram-negative bacteria, such as lipopolysaccharide, can be used to trigger chronic inflammation in microglia (Yu et al., 2022). Jung et al. (2023) conducted a study on mice given lipopolysaccharide (LPS), demonstrating through behavioral tests that microglia increased their activity in the presence of LPS and that the mice exhibited cognitive decline.

Other immune system cells are also involved in neuroinflammation in AD, such as astrocytes, monocytes, and macrophages. Astrocytes maintain BBB integrity and are responsible for ion balance, which plays a crucial role in synaptic communication and neurotransmission in neurons (Romeo et al., 2021). They are cells that can change their morphology. In AD, the accumulation of Aβ and pTau proteins in the brain causes astrocytes to become reactive (Dai et al., 2023). Because their over reactivity causes a prolonged proinflammatory response, they also produce neurotoxic effects by secreting IL-6 and TNF-α cytokines. As a result of the neurotoxic effect, the BBB may be disrupted, allowing monocytes and macrophages to enter the brain from the circulatory system (Zhang & Jiang, 2015). While all these responses initially provide a protective effect, the longer the proinflammatory response, the progression of AD, and therefore neuronal damage, continues (Li et al., 2018).

This thesis aims to develop 2D and 3D *in vitro* models that more realistically reflect AD.

In the first phase, both 2D and 3D AD models will be created using only the SHSY5Y cell line in the presence of $A\beta_{1-42}$. In the second phase, the model's complexity will be increased by incorporating the N9 cell line, which represents microglial cells, into the system, and adding LPS to the medium to stimulate microglial activation. In this context, an AD model will be developed for the first time in which SHSY5Y and N9 cells are co-cultured in a 3D Petri Dish®.

This study aims to develop a 3D engineering-based *in vitro* AD model that is relatively low-cost, easy to use, produces rapid results, and better mimics physiological conditions. The developed model is expected to enable a better understanding of the molecular mechanisms of Alzheimer's disease, the testing of therapeutic agents in a more realistic microenvironment, and its use as a high-throughput screening platform in new drug development. Furthermore, this thesis aims to systematically evaluate the effects of microglia on Alzheimer's pathophysiology *in vitro*.

SECTION TWO

2.MATERIALS & METHODS

2.1 Study Design

The design and methods used in this study are given schematically in the Figure 4.

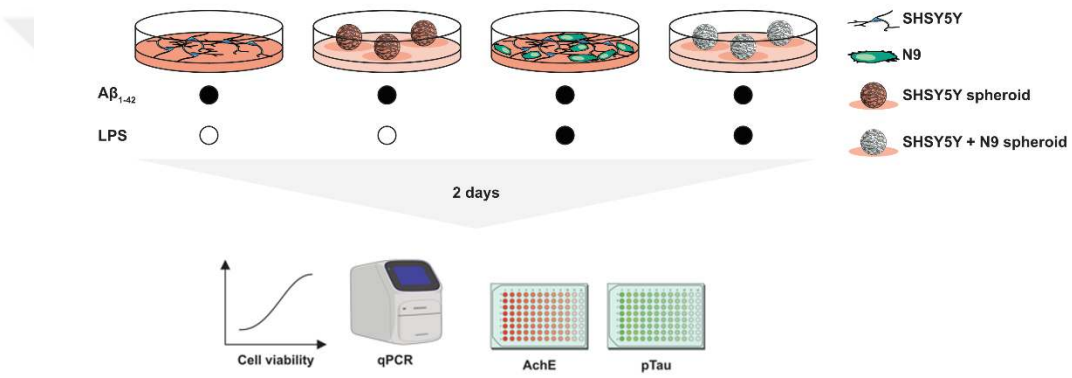

Figure 4: Schematic representation of experimental design

In this study, First, 2D and 3D Alzheimer's disease models were developed using the SHSY5Y cell line. During this phase, a pathological environment was created by adding the $A\beta_{1-42}$ peptide to the medium, and the model's validity was confirmed with various tests. Cell viability was determined using the Alamar Blue™ assay. Furthermore, the Alzheimer's model was characterized using biochemical markers such as acetylcholinesterase (AChE) activity, phosphorylated Tau (p-Tau), and protein levels. Thus, monoculture models reflecting the fundamental neurodegenerative features of Alzheimer's disease were obtained.

Next, to understand the neuroinflammatory process in Alzheimer's disease, SHSY5Y cells were cocultured with N9 microglia cells. Similarly, coculture models

were developed first in a 2D environment and then in a 3D culture system. In this phase, neuroinflammatory responses associated with Alzheimer's pathology were evaluated in models involving neuron-microglia interactions. Neurodegenerative changes were also examined by measuring p-Tau expression and AChE activity. Thus, Alzheimer's disease models have been expanded to encompass not only neuronal degeneration but also its immunological aspects.

In addition, the expression of genes that play a critical role in the pathophysiology of Alzheimer's disease was also included in the characterization process. For this purpose, expression levels of *APP, ADAM9, BACE1, MAPT, AChE, BDNF* and *CREB* genes were analyzed using quantitative real-time polymerase chain reaction (qRT-PCR). 2D and 3D Alzheimer's disease models were comprehensively evaluated in detail from biochemical, molecular and genetic perspectives.

2.1. Cultivation, Passaging and Stocking of SHSY5Y and N9 Cells

SHSY5Y cell line obtained from Ege University Bioengineering Department EBIOPHASE laboratory was cultivated with DMEM high glucose (DMEM HG, Sigma-Aldrich, Lot: RNBN2208) medium containing 10% fetal bovine serum (FBS, Sigma-Aldrich, Lot: 0001689456) and 0.1% gentamicin (Capricorn, Lot: CP21-4333) at 37°C, 5% CO_2, 95% humidity.

N9 cells were cultured in RPMI (Sigma-Aldrich, Lot: RNBG3769) medium containing 10% FBS, and 0.1% penicillin-streptomycin at 37°C in a 5% CO_2, 95% humidity incubator.

The cultures mediums were changed every two days. SHSY5Y cells were separated from the surface using 0.25% trypsin/EDTA (Euroclone, Lot: EUM021) solution when they reached 90% confluency and were transferred to new cell culture dishes and multiplied. The multiplied cells were also taken to a freezing medium containing 10% Dimethylsulfoxide (DMSO, AppliChem, Lot:4Y017835) and 90% FBS and first frozen at -86℃ overnight and then transferred to liquid nitrogen at -196℃ for long-term storage. Thus, a master stock was created for the cells and then a working stock was prepared to continue the studies at the same passage number.

2.2 Engineered Model of AD Disease

2.2.1 Preparation of $A\beta_{1-42}$ Peptide Stock

Commercially available $A\beta_{1-42}$ (Sigma-Aldrich, A9810) peptide was dissolved in sterile, cell culture-friendly DMSO at a concentration of 4 μM according to the manufacturer's instructions. The $A\beta_{1-42}$ dissolved in DMSO was then aliquoted and stored at -20°C.

2.2.2 Development of 2D AD Model

The prepared $A\beta_{1-42}$ stock was first tested on SHSY5Y cells in 2D using the following method to create an AD model;

- The $A\beta_{1-42}$ peptide was removed from the stock at -20℃ and then kept at 37 ºC for 5 days at the incubator (Yamamoto et al., 2004).
- Then, the $A\beta_{1-42}$ peptide was added to the DMEM HG medium and kept at 37ºC for 1 day to ensure fibrillation and to obtain soluble fibril formation of $A\beta_{1-42}$ (Mensinger et al., 2020).
- SHSY5Y cells were cultured in 96 well plate with DMEM HG which contains 10% FBS, 1% L-glutamine, and 0.1% gentamicin at a concentration of $5x10^4$ cells/mL.
- $A\beta_{1-42}$ peptide was applied to the cells with a serial dilution method with an initial concentration of 8 μM 24 hours after the cells adhered to the surface.
- In the Alzheimer's disease model, the presence of the $A\beta_{1-42}$ peptide, which is a toxic form for cells, causes a decrease in cell viability. Therefore, in order to find the optimum amount of $A\beta_{1-42}$ peptide for the AD model, cell viability test was performed with Alamar Blue™ assay. The $A\beta_{1-42}$ peptide concentration that observed a significant decrease in cell viability in the AD model was accepted as the appropriate amount for AD.
- SHSY5Y cells were incubated with media containing $A\beta_{1-42}$ peptide at the concentration given above for 24, 48 and hours.
- At the end of the 24th, 48th and 72th hours, Alamar Blue™ Assay was performed.

2.2.3 Development of 3D AD Model

- The 3D "Petri Dish® (MicroTissues Inc. USA)" method was used to create 3D microtissues (Gong et al., 2015). For the creation of molds and 3D gels, a 3% (w/v) agar (Sigma-Aldrich, A1296-100G) solution containing 0.1% (w/v) NaCl was sterilized in an autoclave at 121°C and 1.02 atm pressure for 30 minutes.
- 330 μL of the sterile agar solution was placed in the chamber of the mold and the agar was waited for gelation. After gelation, the mold was turned upside down and the 3D non-adhesive agar gel, where the microtissues would be created, was placed in a 24-well culture dish. Agar gels were conditioned in a nutrient medium at 37°C and 5% CO_2 in a 95% humidity incubator for 30 minutes before cell cultivation.
- After conditioning, SHSY5Y cells were seeded into each of the microtissue mold at a density of 7×10^6 cells/mL, allowing microtissues to form for 24 hours.
- After 24 hours, the upper phase of the formed microtissues was taken, and the $A\beta_{1-42}$ peptide was added at an initial concentration of 20 μM, and the serial dilution method was applied.
- Subsequently, the Alamar Blue™ assay was performed to find the variationin cell viability and the optimum amount of $A\beta_{1-42}$.

2.2.4 2D *in vitro* Co-Culture AD Model

The cell lines cultivated were SHSY5Y and the N9 cell line. Cultivation conditions and adaptation processes to DMEM HG media described in the section 2.2.4.1 and 2.2.4.2.

2.2.4.1 Growth Kinetics of N9 Cells

- Cells were detached with 0.25% trypsin-EDTA solution when confluence reached 80–90%. Then, they were seeded into 96-well plates at densities of 10^3 cells/mL, $5x10^3$ cells/mL, 10^4 cells/mL, $5x10^4$ cells/mL, 10^5

cells/mL, $5x10^5$ cells/mL, and 10^6 cells/mL for 14 days. After waiting 24 hours for the cells to attach, their growth behavior was observed daily using 3-(4,5-Dimethylthiazol-2-yl)-2,5-Diphenyltetrazolium Bromide (MTT) (Sigma-Aldrich, Lot: M5655) analysis until day 14.

- At the end of the specified incubation periods, serum-free RPMI medium containing 10% (v/v) MTT solution was added to each well, and the cells were incubated for an additional 3 hours at 37°C, 5% CO_2.
- Subsequently, the MTT-containing medium was removed, and Dimethylsulfoxide (DMSO) was added to the wells to dissolve the formed formazan crystals.
- Absorbances were measured at 570 nm and 690 nm wavelengths on a spectrophotometer.
- To obtain viability results and eliminate background absorbance values, the 690 nm data were subtracted from the 570 nm data.
- After generating the growth graph, the cell concentration indicating adaptation, logarithmic, stationary, and death phases was selected.

2.2.4.2 Adaptation of N9 Cells to Co-Culture Medium

- Optimizing the growth media of SHSY5Y and N9 cell lines is crucial for co-culture.
- After determining the growth kinetics of N9 cells cultivated in the original medium, the cells were gradually transferred to the DMEM HG medium to be used for co-culture.
- After this step, a gradual transition from RMPI medium to DMEM HG was achieved. Initially, the RPMI: DMEM HG ratio was 75:25, and cells were gradually passaged until the ratio reached 0:100.
- After the cells were fully adapted to DMEM HG, their behavior was monitored for 14 days in DMEM HG at a concentration of $5x10^3$ cells/mL. This can be seen in Figure 9.

2.2.4.3 Development of a 2D *in vitro* Co-Culture AD Model

- To establish a 2D *in vitro* AD model, the co-culture behavior of SHSY5Y and N9 cells was first examined. For this purpose, SHSY5Y:N9 cells were seeded into 48-well plates at SHSY5Y:N9 ratios of 2:1, 1:1, 1:2, and 2:2.
- Cell behavior was monitored for 3 days. Based on the results, it was decided to continue with the 1:2 SHSY5Y:N9 ratio.
- To develop the co-culture AD model, cells seeded at a 1:2 ratio and incubated at 37°C, 5% CO_2 for 3 days.
- At the end of the 3 days, the cells were incubated with DMEM HG medium containing $A\beta_{1-42}$ using a serial dilution method, containing 10 µM and 1 mg/mL LPS (He et al., 2016).
- Alamar Blue™ analysis was performed after 48 hours.

2.2.5 Development of a 3D *in vitro* Co-Culture AD Model

- The 3D Petri Dish® (MicroTissues Inc. USA) method was used to create 3D microtissues (Gong et al., 2015).
- For 3D microtissue production, 3% (w/v) agar solution containing 0.1% (w/v) NaCl was prepared and sterilized in an autoclave at 121°C and 1.02 atm pressure for 30 minutes.
- 330 µL of sterile agar solution was placed in the mold chamber and allowed to mold formation.
- After a time, the mold was inverted, and the 3D agar gel, from which the microtissues would be created, was placed in a 24-well culture dish.
- The agar gels were conditioned by incubating them in the nutrient medium in an incubator at 37°C and 5% CO_2, with 95% humidity, for 30 minutes before cell seeding.
- Following the conditioning step, SHSY5Y and N9 cells were seeded into micromolds at a 1:2 ratio (SHSY5Y cells $2.33x10^6$ cells/mL and N9 cells $4.67x10^6$ cells/mL, 35 µL each).
- At the end of 24 hours following cell seeding, the medium on the cells was replaced with medium containing 1 mg/mL LPS and serially diluted Aβ1-42, starting with a 20 µM initial concentration.

- Alamar Blue™ Analysis was performed after 48 hours of incubation.

2.3 Characterization of AD Model

2.3.1 Alamar Blue™ Assay

The Alamar Blue™ Assay (Invitrogen, Lot:2359067) is a calorimetric test that indicates cellular viability and metabolic activity. A decrease in cell viability is expected in the AD model (Rampersad, 2012; Stephenson et al., 2013; Rezai-Rad et al., 2015). The Alamar Blue™ Assay described below was performed in the same manner for both co-culture and monoculture.

Alamar Blue™ Assay in 2D AD Model:

- The medium on the cells is first removed.
- Serum-free medium which contains 10% Alamar Blue™ dye was added to the cells.
- The cells were incubated at 37°C, 5% CO_2 in the dark for 4 hours.
- At the end of 4 hours, absorbance was measured with a spectrophotometer at 570 and 600 nm wavelengths.
- To eliminate background absorbance, raw data is obtained by subtracting the 600 nm wavelength from the 570 nm wavelength.

Alamar Blue™ Assay in 3D AD Model:

Harvesting microtissues step is crucial to accurate assess cell viability. Therefore, a method was developed based on the microtissue harvesting performed by Dogan (2017) and the Alamar Blue™ test was performed.

- To determine cell viability, agar micro tissue molds were inverted with sterile forceps. Then, they were centrifuged for 5 minutes, 1000 rpm and 4 ºC.
- The medium containing the micro tissues was transferred to the eppendorf tube. In order for the micro tissues to come together and form a pellet, the tubes were centrifuged for 5 minutes at 1000 rpm.
- The supernatant was removed.

- A total volume of 150 µL of medium containing 10% Alamar Blue^{TM} dye and 90% serum-free medium was added to each eppendorf tube and the pellets were dispersed.
- 150 µL of each sample was added to the 96-well plate and plate was incubated at 37°C, 5% CO_2 for 4 hours.
- After 4 hours of incubation, the samples were taken back into the eppendorf tube and centrifuged for 5 minutes at 1000 rpm.
- A 100 µL volume of sample from each tube was added into a 96-well plate.
- Viability analysis results were obtained in a spectrophotometer at a wavelength of 570-600 nm.
- To eliminate background absorbance, raw data is obtained by subtracting the 600 nm wavelength from the 570 nm wavelength.

2.3.2 Quantitative Real Time Polymerase Chain Reaction (qRT-PCR)

Polymerase Chain Reaction is the process of multiplying RNA obtained from samples such as cells and tissues by converting it into cDNA (Shiao, 2003).

- First, the AD model was created for the polymerase chain reaction (PCR).
- Then, the cells were harvested.
- To harvest the cells, the following steps were followed in order:
- The supernatant of the cells was thrown away.
- The cells were gently washed with Ca^{+2}, Mg^{+2} free PBS.
- The cells were separated from the well plate with 0.25% trypsin-EDTA.
- Subsequently, the medium was added to dilute the trypsin-EDTA and the cells were collected in an eppenforf tube.
- Cells were centrifuged at 1000 rpm for 5 minutes.
- At this stage, the step of obtaining total Ribonucleic Acid (RNA) isolation was started.
- RNA isolation kit (Lucigen, MC85200) was used for total RNA isolation.
- Cells were treated with lysis and protein precipitation solution.

- RNA was precipitated with isopropanol, washed with 70% ethanol, and vortexed.
- Absorbances at 260 nm and 280 nm wavelengths were measured to determine the concentration and purity of isolated RNA.
- The isolated total RNAs were used in complementary Deoxyribose Nucleic Acid (cDNA) synthesis as at least 3 µg.
- The cDNAs obtained as a result of the synthesis were diluted with nuclease-free water at a ratio of 1:4 and used for qRT-PCR processes.
- For the synthesis of cDNA, RNAs which A260/A280 ratios between 1.8-2 were selected and then cDNA synthesis procedure (Applied Biological Materials-abm Inc, G236) performed.
- Changes in mRNA expression levels of genes were affecting AD such as *ADAM9, APP, BACE1, MAPT*, *ACHE, CHAT*, *BDNF* and *CREB* genes were investigated with qRT-PCR.
- For real-time *PCR, ADAM9, APP, BACE1, MAPT, ACHE, CHAT, BDNF, CREB* and *βACT* (beta actin) primers were diluted to 10 µM.
- 1 µL of diluted cDNA, 0.5 µL of 10 µM forward (F) and reverse (R) primers were mixed with 8 µL of nuclease-free water and 10 µL of SYBR Green mixture (Applied Biological Materials-abm Inc, G891) was added.
- Initial denaturation was performed at 95 °C for 3 minutes, followed by a total of 40 cycles; PCR program was created to denaturate at 95 °C for 15 seconds, annealing and chain extension at 60 °C for 1 minute.
- For the melting curve analysis, another segment was added at the end of the 40th cycle for 1 minute at 95 °C, 30 seconds at 55 °C and 30 seconds at 95 °C.
- The presence and purity of PCR products were checked with melting curve analyses.
- In the analysis of the expression levels of gene products, β-Act was used as the reference gene and relative mRNA expression levels were calculated compared to the control group using the "Comparative ΔΔCT" method.

2.3.3 Bicinchoninic Acid (BCA) Assay

Bicinchoninic Acid Assay (BCA) is a colorimetric method that allows determining the protein concentration in biological samples such as cells and tissues (Olson and Markwell, 2007).

- To perform BCA assay (Thermo Scientific, 2327), firstly the cells are harvested and lysed.
- The methods of lysed cells in 2D and 3D AD models are different from each other. For 2D AD model, first the upper phase of the cells was discarded. Then the cells were washed with Ca^{+2}, Mg^{+2} free PBS.
- Cells were separated from the plate surface with the help of trypsin-EDTA.
- DMEM HG was added to the cells separated from the surface and they were collected in an eppendorf tube.
- In the AD model created with the 3D microtissue method, the microtissue molds were turned upside down with the help of sterile forceps.
- The plate was centrifuged for 5 minutes at 1000 rpm.
- Then the cells in each mold were collected and placed in an eppendorf tube.
- After these steps, each process was continued as follows in the 2D and 3D AD models.
- Harvested cells were centrifuged for 5 minutes at 1000 rpm.
- The medium was removed from tubes. It was washed again with Ca^{+2}, Mg^{+2} free PBS.
- Lysis buffer was added to each eppendorf tube.
- The cells were sonicated with a sonicator for 30 minute.
- In order to remove insoluble material, the tubes were centrifuged again after the sonication process.
- The supernatant was taken to a clean eppendorf for use.
- Each sample was kept on ice until the BCA analysis was completed.
- 2mg/mL BSA stock solution was used to create the standard curve of the BCA analysis. Protein contents with known concentrations were obtained by serial dilution.
- Standards and samples were taken into 96 well plates as 25 µL.

- Working reagent (50:1) was created with BCA Protein Assay Reagent A and BCA Protein Assay Reagent B.
- 200 µL was added to each sample and standards.
- After shaking for 30 seconds, it was incubated at 37 ºC for 30 minutes.
- Following incubation period, plate was cooled to room temperature and absorbance values was read at 562 nm on the spectrophotometer.
- A standard curve was generated with absorbances for known protein concentrations.
- According to the standard curve, protein concentrations were obtained from the absorbance values of the samples.

2.3.5 pMAPT/pTau Amount Determination

An increase in the amount of pTau is expected in AD model (Tarasiuk et al., 2018). The following protocol was performed according to the manufacturer's instructions for the pTau ELISA kit (Elabscience, E-BC-K028-M).

- Biotinylated Detection Ab Working Solution, HRP Conjugate Working Solution, Wash Buffer and standards are prepared in the amount to be used.
- 2D and 3D AD models were created. Cells were harvested for the assay as described in the BCA assay.
- Following cell harvesting, 100 µL of standards and samples were added to the 96-well which contains to the samples.
- Incubation was carried out for 90 minutes at 37ºC in a CO_2-free incubator.
- As soon as the liquid was removed from the well after 90 minutes, biotinylated detection Ab working solution was added to each well and the 96 well plate incubated for 1 hour at 37ºC in a CO_2-free incubator.
- At the end of the incubation time, biotinylated detection Ab working Solution was removed from the plate and washed three times with wash buffer.
- Subsequently, 100 µL of HRP conjugate working solution was added to the well containing the samples and incubated for 30 minutes at 37ºC in a CO2-free incubator.

- After removing the liquid medium, the plate was washed five times with wash buffer.
- Once the washing was completed, 90 µL of substrate reagent was added and incubated for 15 minutes at 37ºC in a CO_2-free incubator.
- At the end of 15 minutes, stop solution was added to each well.
- Measurements were immediately taken with a spectrophotometer at a wavelength of 450 nm.

2.3.6 Acethylcholinesterase (AchE) Activity Assay

An increase in AchE levels is expected in the AD model (García-Ayllón et al., 2021). The protocol for this assay was established in accordance with the manufacturer's instructions provided with the kit (Elabsciense, E-BC-K174-M).

- First, AD models in both 2D and 3D formats were constructed.
- Following step, cells were harvested for the assay as described in the BCA assay.
- 200 µL of lysis buffer was added to each eppendorf tube and sonicated for 30 minutes.
- After sonication process, samples were centrifuged for 5 minutes at 1000 rpm.
- The supernatant was transferred to a new eppendorf tube.
- BCA analysis was performed to determine protein concentration ratios before starting the acetylcholine esterase assay.
- Following the BCA analysis, 20 µL of each sample was taken into the plate provided in the kit for the AchE assay.
- Then, 170 µL of chromogenic solution was added, followed by 10 µL of substrate working solution.
- Absorbance measurements were performed in two stages. Before the first measurement, the plate was mixed in the spectrophotometer for 5 seconds. Measurements were taken at 412 nm wavelengths for 30 and 330 seconds to obtain ΔA. The absorbance at 30 seconds was recorded as A_1, and the wavelength at 330 seconds was recorded as A_2.
- AChE levels (U/mL) were quantified according to the following formula:

$$\text{AchE Activity (U/mL)} = \frac{(\Delta A \times \frac{V_{total}}{\varepsilon \times d} \times 10^9) \div (C_{pr} \times V_{sample}) \div T \times f}{Cell\ Viability} = \frac{245 \times \Delta A \div C_{pr} \times f}{Cell\ Viability}$$

$\Delta A = A_2 - A_1$

ε = molar extinction coefficient oSSf TNB, 1.36×10^4 L/mole/cm,

d = optical path of the 96 wells microplate, 0,6 cm,

V_{total} = total volume of reaction system, 2×10^{-4} L,

V_{sample} = volume of sample added into the reaction system, 2×10^{-2} mL,

10^9 = unit conversetion, 1 mol = 10^9 nmole,

T = reaction time, 5 min,

C_{pr} = concentration of protein in sample, mg/mL,

f = diluton factor of sample before test.

SECTION THREE

3. RESULTS

3.1 Alzheimer's Disease Model

3.1.1 2D Alzheimer's Disease Model

Figure 5 shows inverted phase microscope images of SHSY5Y cells treated with $A\beta_{1\text{-}42}$ peptide at 8, 4, and 2 μM for 48 hours. When the images are examined, it is seen that the change in cell form begins after 48 hours at the highest dose.

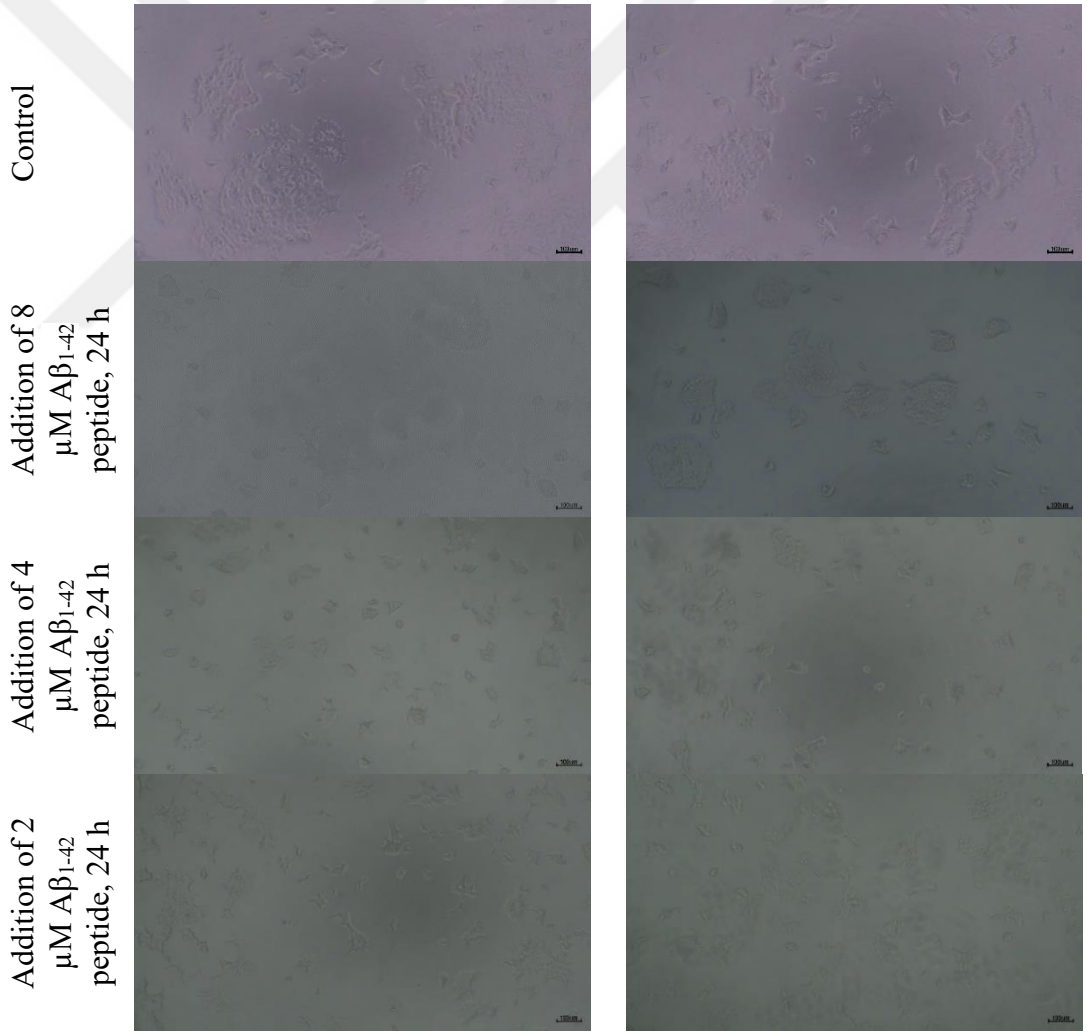

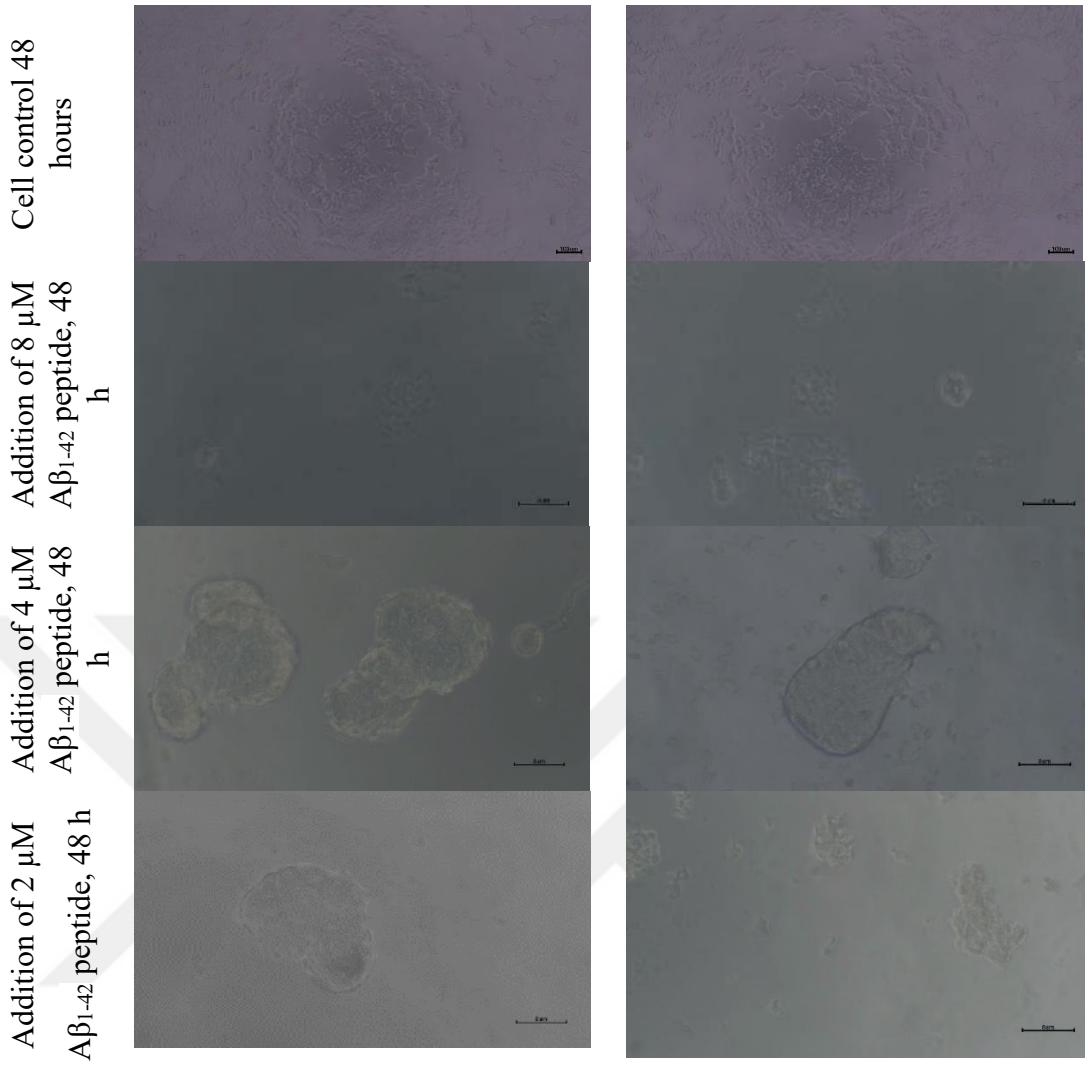

Figure 5: 2D Alzheimer's Disease Model Experimental Images at different $A\beta_{1-42}$ concentrations and on different days (4X magnification, Olympus CK40)

3.1.2 3D Alzheimer's Disease Model

Inverted phase microscope images at 10X magnification of microtissues treated with 20-0.625 µM $A\beta_{1-42}$ peptide for 48 hours are shown in Figure 6. The phenomenon observed here is similar to that observed under 2D conditions. Spheroid disintegration began at 48 hours and at the highest dose of 20 µM. The structural integrity of the spheroids appears to be preserved as the dose decreases.

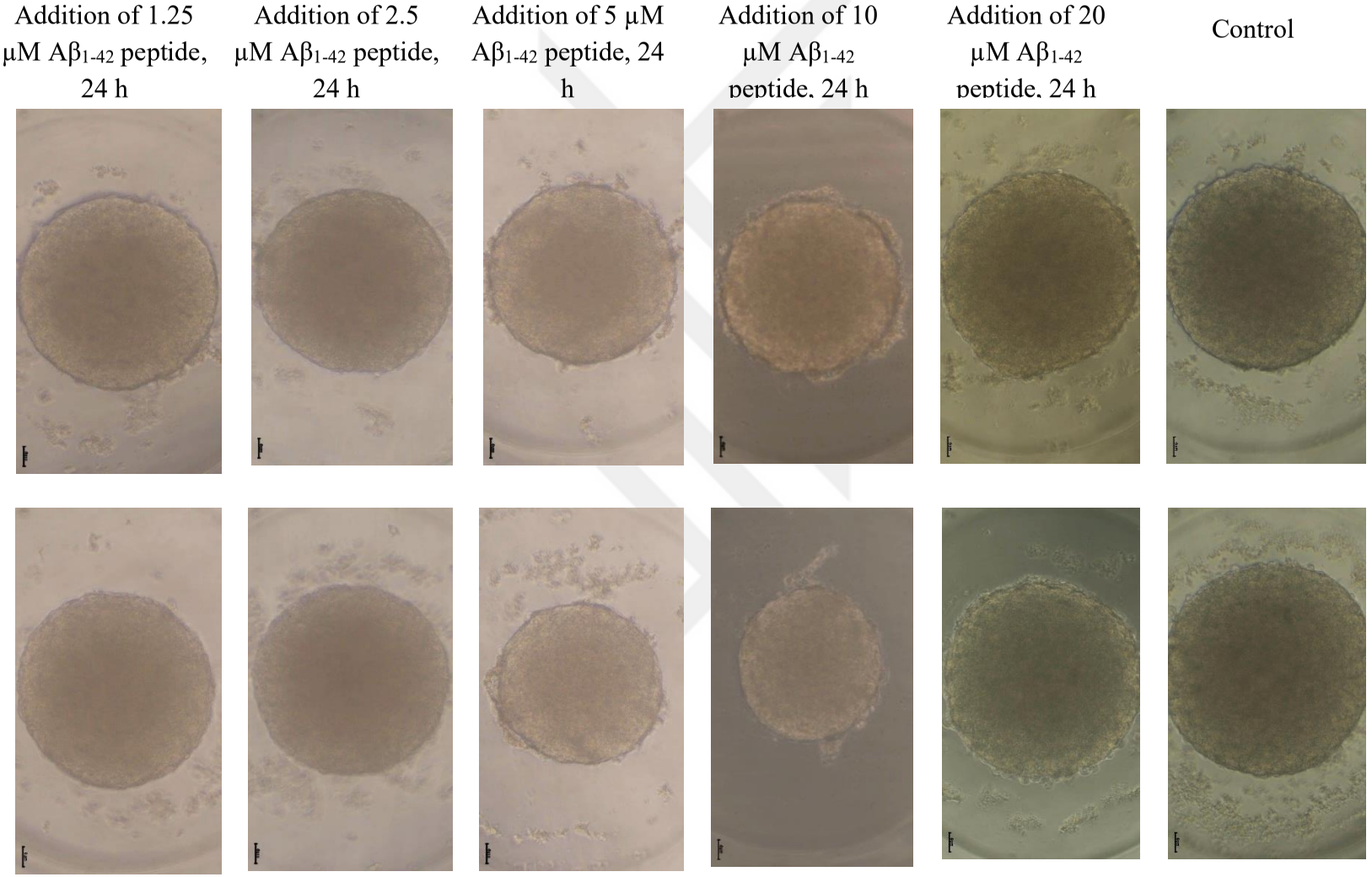
Addition of 1.25 µM Aβ1-42 peptide, 24 h
Addition of 2.5 µM Aβ1-42 peptide, 24 h
Addition of 5 µM Aβ1-42 peptide, 24 h
Addition of 10 µM Aβ1-42 peptide, 24 h
Addition of 20 µM Aβ1-42 peptide, 24 h
Control

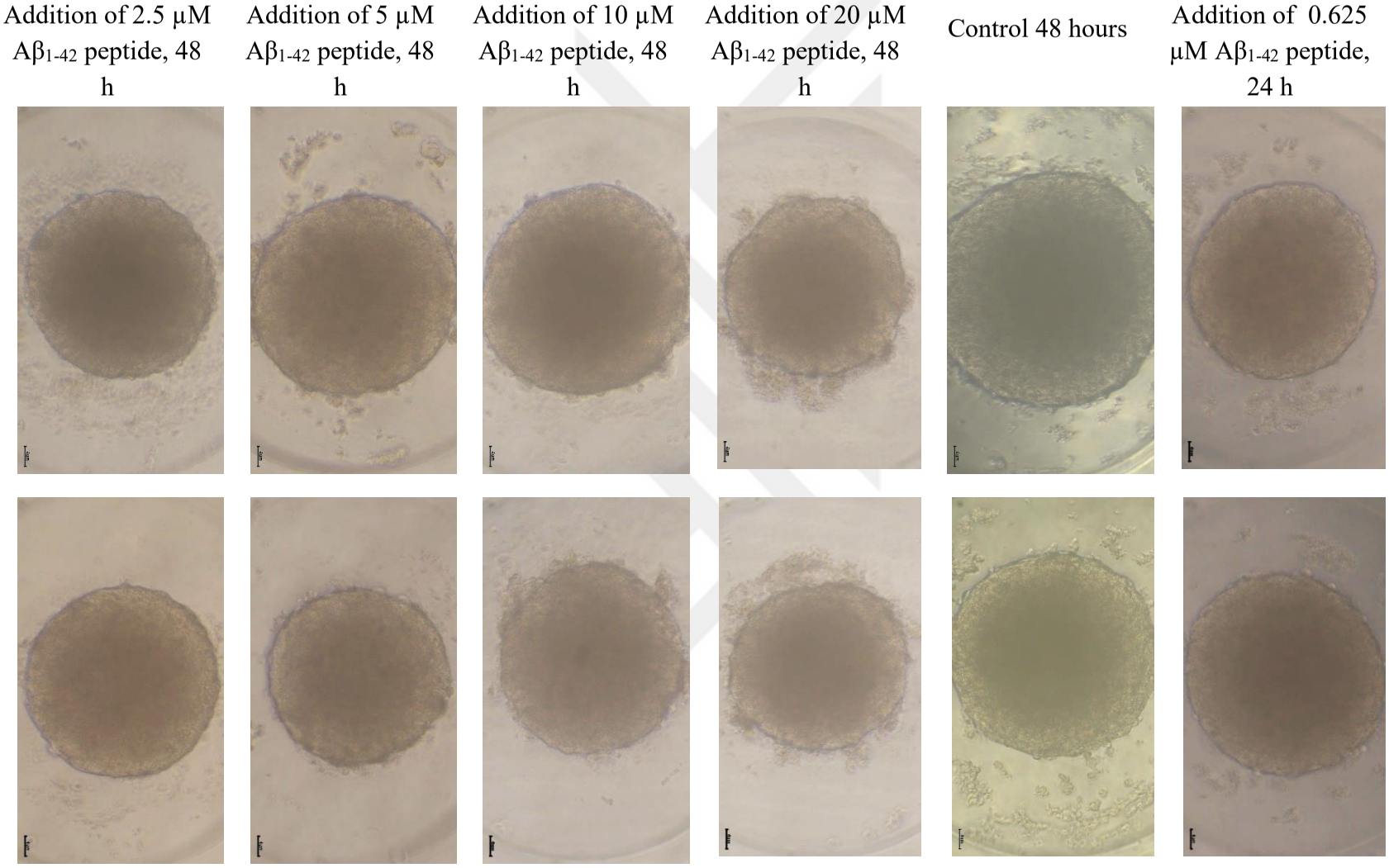
Addition of 2.5 µM Aβ1-42 peptide, 48 h
Addition of 5 µM Aβ1-42 peptide, 48 h
Addition of 10 µM Aβ1-42 peptide, 48 h
Addition of 20 µM Aβ1-42 peptide, 48 h
Control 48 hours
Addition of 0.625 µM Aβ1-42 peptide, 24 h

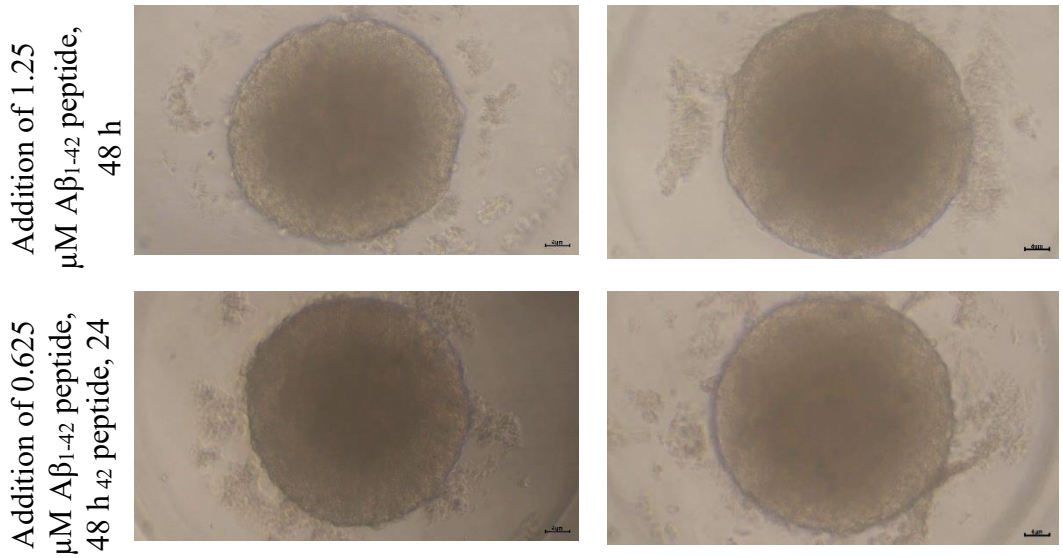

Figure 6: 3D Alzheimer's Disease Model Experimental Images at different $A\beta_{1-42}$ concentrations and on different days (10X magnification, Olympus CK40)

3.1.3 Co-culture 2D Alzheimer's Disease Model

3.1.3.1 N9 Growth Kinetics

The N9 cell line is a gift from the Genc Laboratory of the Izmir Biomedicine and Genome Center. Because the cells brought to the laboratory from abroad and the SHSY5Y cell line to be cocultured were in a different medium, the growth kinetics of the cell were studied for adaptation.

3.1.3.2 Growth Kinetics of N9 Cells in RPMI Medium

The growth behavior of N9 cells was observed in RPMI medium at different concentrations for 14 days. Spectrophotometric measurements were taken at 570 and 690 nm wavelengths for MTT analysis, and the 690 nm wavelength was subtracted from the 570 nm wavelength to remove background absorbance The results are shown in Figure 7 below.

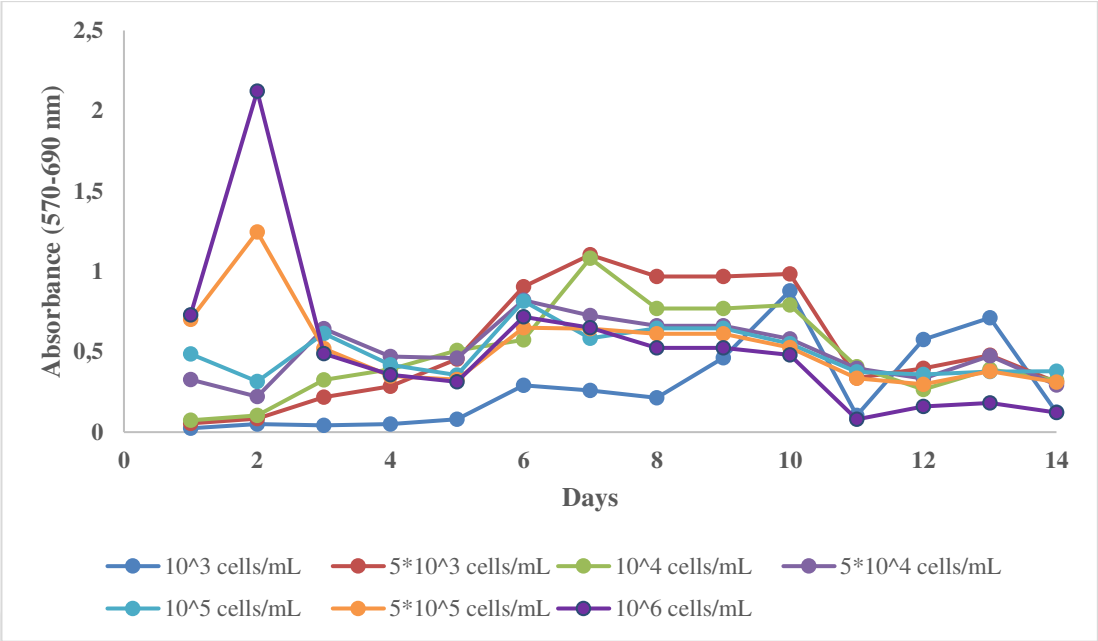

Figure 7: Growth Kinetics Results of N9 Cells in RPMI Medium

Since lag phase, log phase, stationary phase and death phase were observed, the cell density selected for acclimation to DMEM HG medium was $5x10^3$ cells/mL.

3.1.3.3 Growth Kinetics of N9 Cells in DMEM HG Medium

After adapting N9 cells to DMEM HG medium, MTT analysis was performed for 14 days to observe their behavior. Spectrophotometric measurements were taken at 570 and 690 nm wavelengths for MTT analysis, and the 690 nm wavelength was subtracted from the 570 nm wavelength to remove background absorbance. The results are shown in Figure 8.

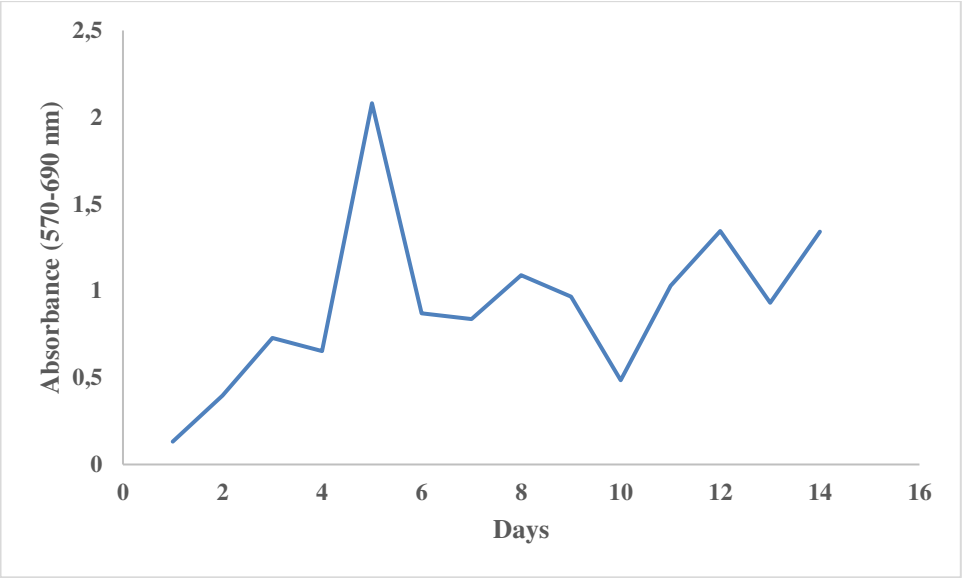

Figure 8: Growth Kinetics Result of N9 Cells in DMEM HG Medium

3.1.3.4 Coculture Results of SHSY5Y and N9 Cells

The results of the MTT test, performed to see which ratios of SHSY5Y and N9 cells create a healthier growth environment, are shown in Figure 9. Based on the results, the cell ratio determined for the appropriate coculture was selected as $5x10^3$ cells/mL:10^4 cells/mL(1:2) ratio for SHSY5Y:N9.

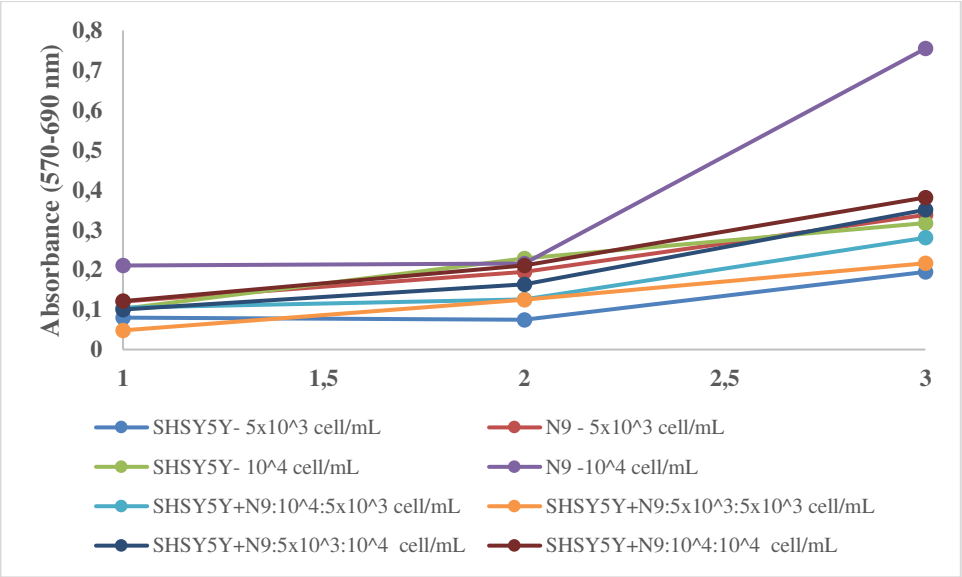

Figure 9: Coculture Results of SHSY5Y and N9 Cells

Figure 10 shows inverted phase microscope images of an *in vitro* co-culture model of N9 and SHSY5Y cells using 1 mg/mL LPS and 10 μM $A\beta_{1-42}$ peptide and its serial dilutions to create a 2D AD model.These observations suggest that, compared to the control group, when the $A\beta_{1-42}$ peptide dose was high, the N9 ratio in the medium increased significantly, and SHSY5Y cells became undetectable in the culture medium.

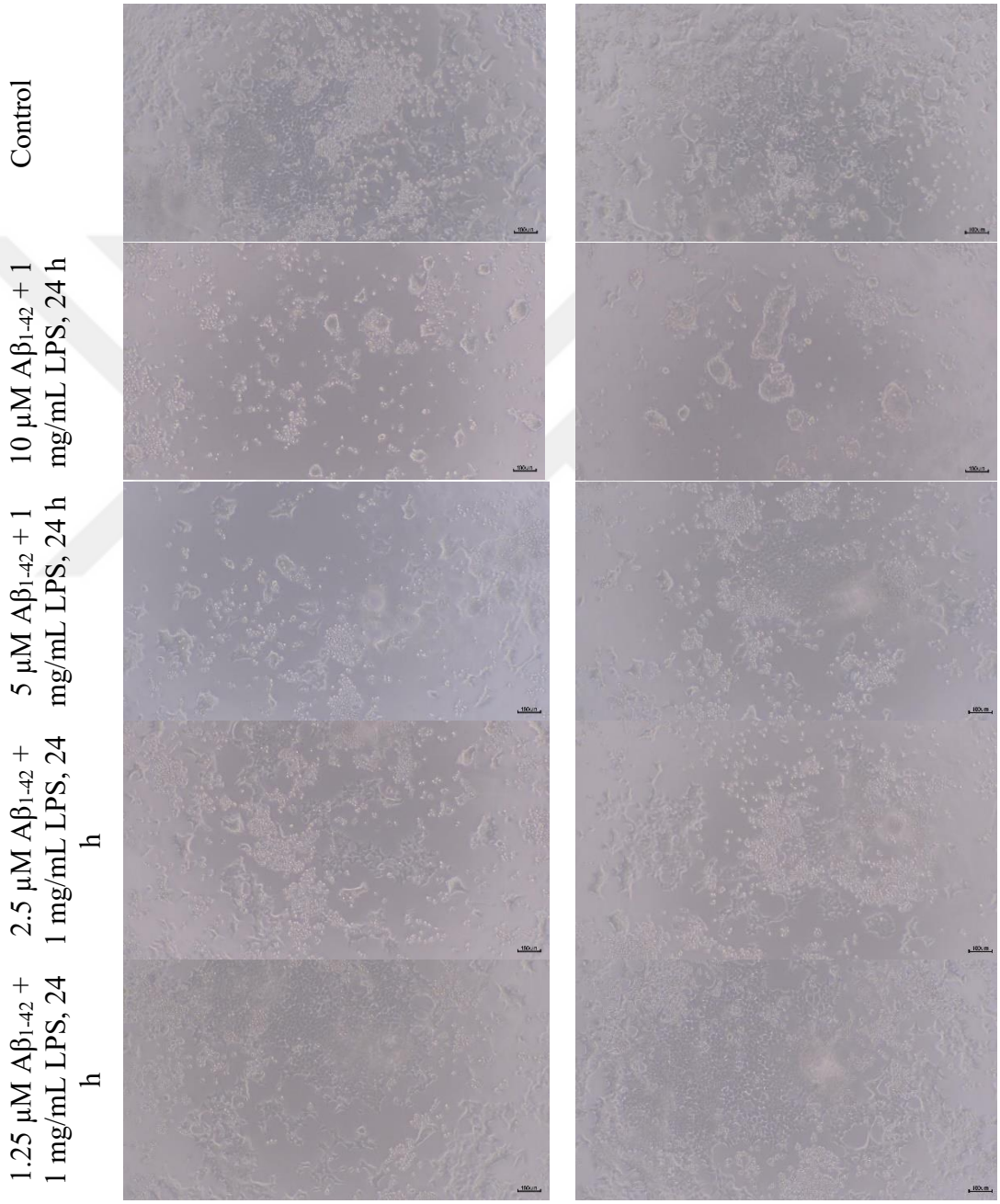

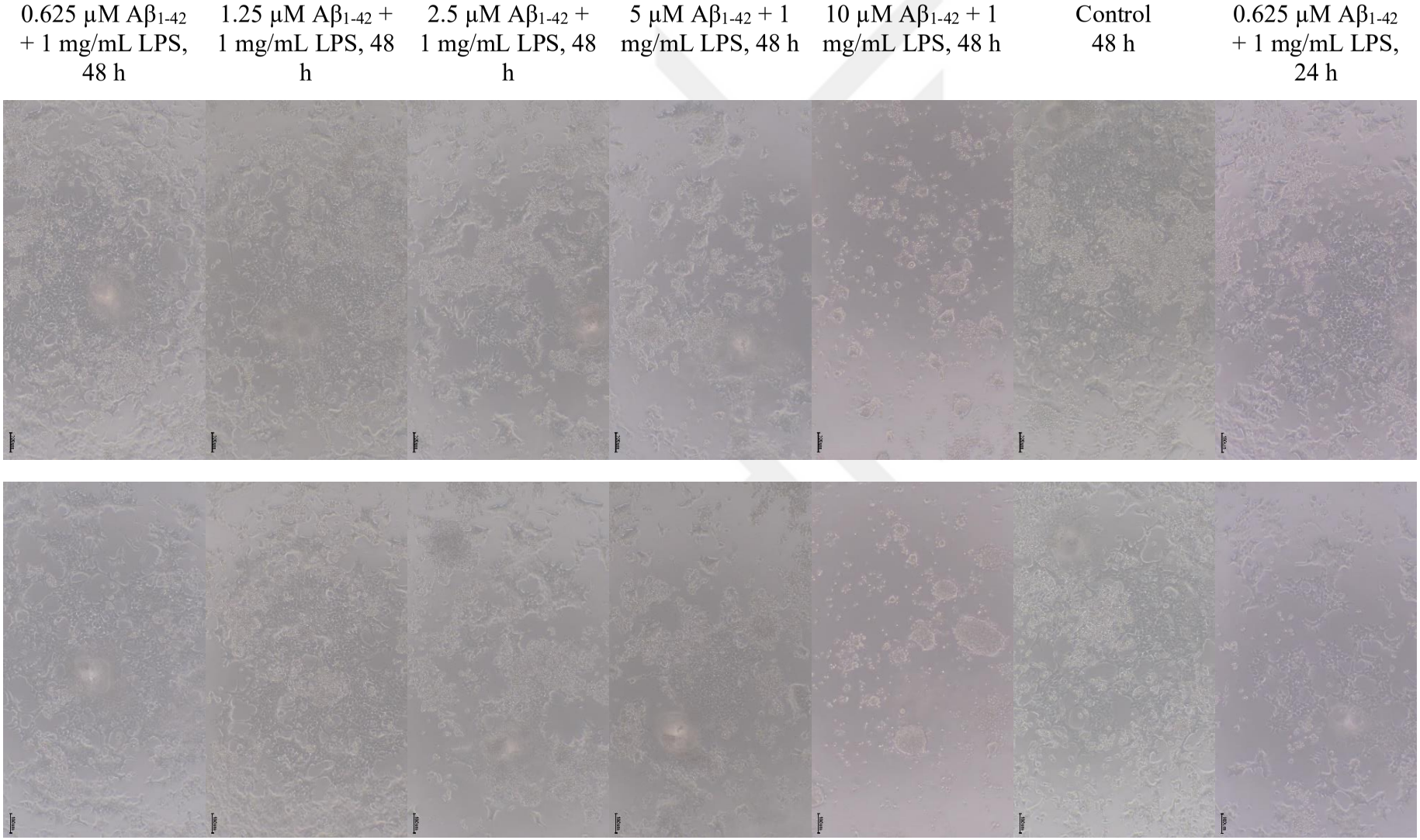
0.625 µM Aβ1-42 + 1 mg/mL LPS, 48 h
1.25 µM Aβ1-42 + 1 mg/mL LPS, 48 h
2.5 µM Aβ1-42 + 1 mg/mL LPS, 48 h
5 µM Aβ1-42 + 1 mg/mL LPS, 48 h
10 µM Aβ1-42 + 1 mg/mL LPS, 48 h
Control 48 h
0.625 µM Aβ1-42 + 1 mg/mL LPS, 24 h

Figure 10: Experimental Images of 2D Coculture Alzheimer's Disease Model at Different $A\beta_{1-42}$ Concentrations and Different Days (4X magnification, Olympus CK40)

3.1.4 Co-culture 3D Alzheimer's Disease Model

The appearance of N9 and SHSY5Y cells co-cultured using the 3D Petri Dish method is quite different from the images obtained from the AH model created with SHSY5Y cells alone. To create the model, microtissues were also incubated in medium containing 20 µM $A\beta_{1-42}$ and 1 mg/mL LPS for 48 hours. However, even in the control group, the tissues failed to develop structural integrity, and the cells were observed to be more dispersed, particularly in the 20 µM $A\beta_{1-42}$ + 1 mg/mL LPS and 48-hour group.

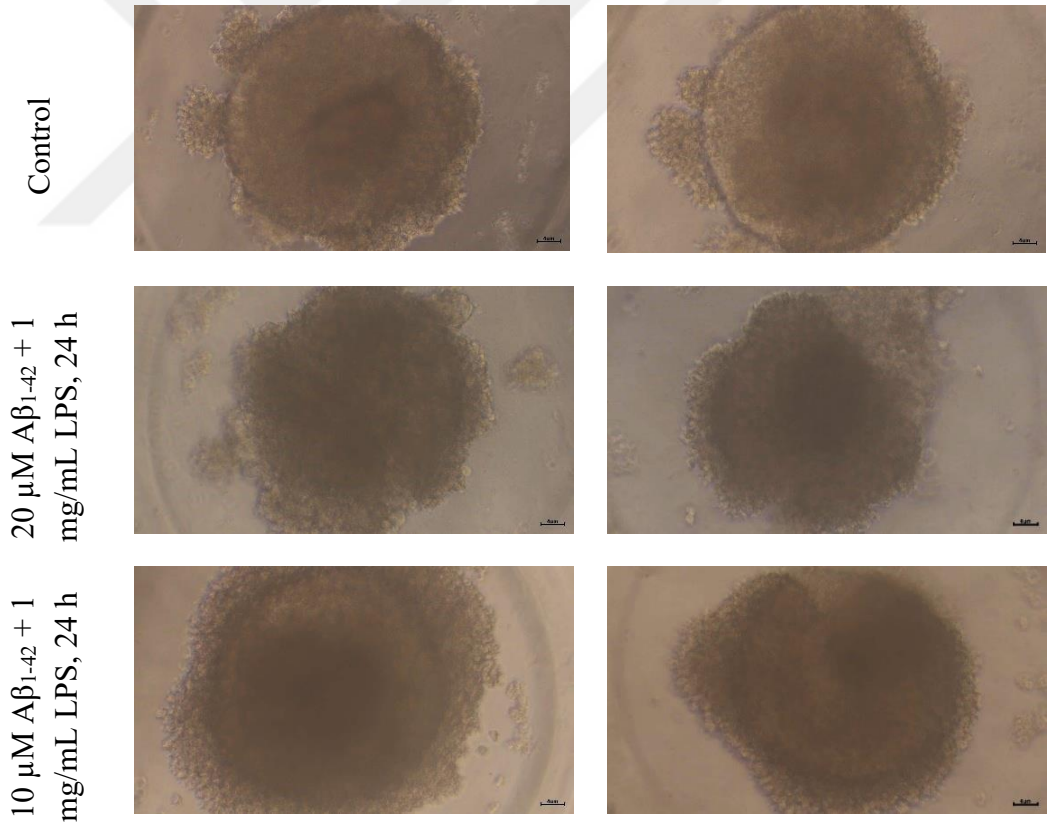

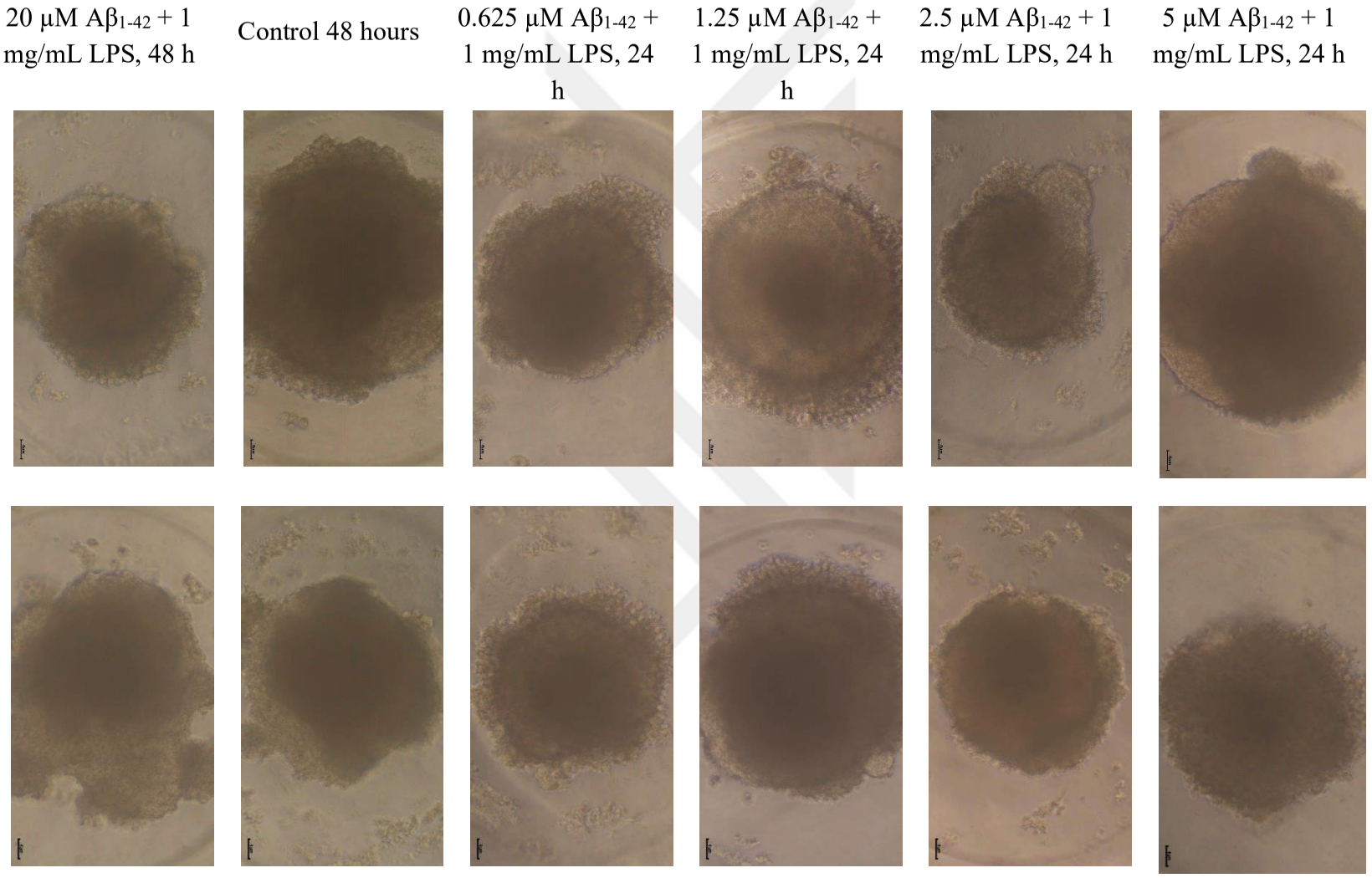
20 µM Aβ1-42 + 1 mg/mL LPS, 48 h
Control 48 hours
0.625 µM Aβ1-42 + 1 mg/mL LPS, 24 h
1.25 µM Aβ1-42 + 1 mg/mL LPS, 24 h
2.5 µM Aβ1-42 + 1 mg/mL LPS, 24 h
5 µM Aβ1-42 + 1 mg/mL LPS, 24 h

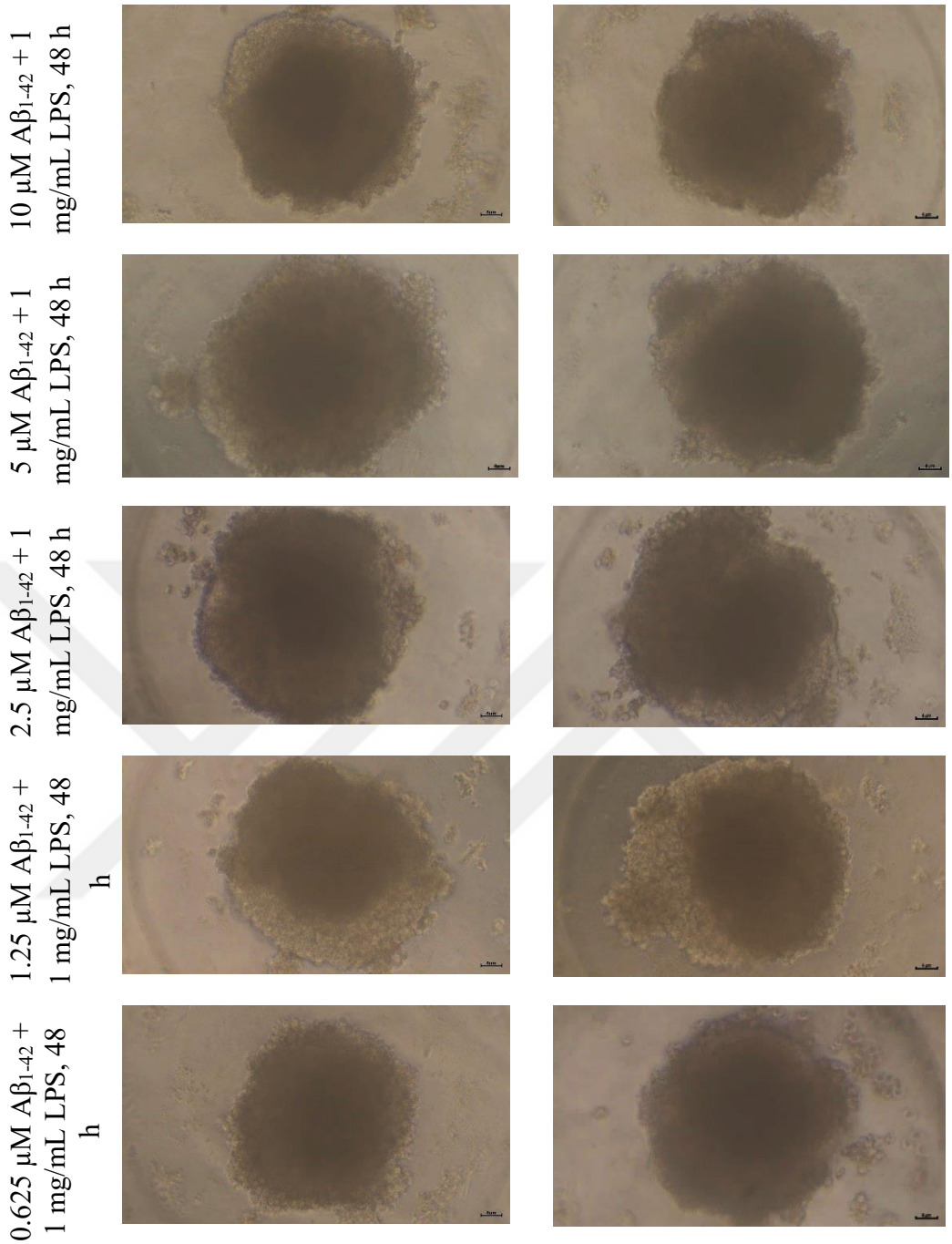

Figure 11: Experimental Images of 3D Coculture Alzheimer's Disease Model at Different $A\beta_{1\text{-}42}$ Concentrations and Different Days (10X magnification, Olympus CK40)

3.2 Cell Viability

The results of the Alamar Blue™ Analysis performed at wavelengths of 570-600 nm are given in Figure 12, 13, 14, 15, 16, 17 and 18. It was determined that the data showed normal distribution and statistical analyses were performed using the one-way ANOVA method.

3.2.1 2D Cell Viability

The optimum $A\beta_{1-42}$ concentration found in the 2D monoculture AD model was 4 µM at 48 hours incubation.

Incubation of SHSY5Y cells with $A\beta_{1-42}$ peptide for 24 hours did not cause any significant change in cell viability. It shown in the Figure 12.

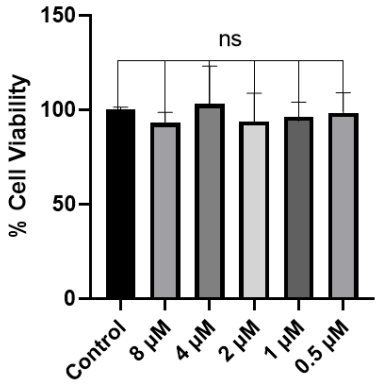

Figure 12: Cell viability data after 24 hours of incubation to determine the optimum $A\beta_{1-42}$ peptide concentration in a 2D AD model

After 48 hours of incubation with $A\beta_{1-42}$ peptide, the viability of SHSY5Y cells was statistically significantly decreased (**$p \leq 0.01$) at 8 µM (Figure 13).

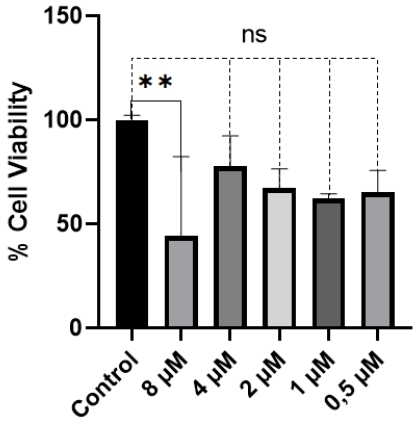

Figure 13 : Cell viability data after 48 hours of incubation to determine the optimum $A\beta_{1-42}$ peptide concentration in a 2D AD model

After 72 hours of incubation with $A\beta_{1-42}$ peptide, the viability of SHSY5Y cells was statistically significantly decreased (****$p \leq 0.01$) at 8 µM (Figure 14).

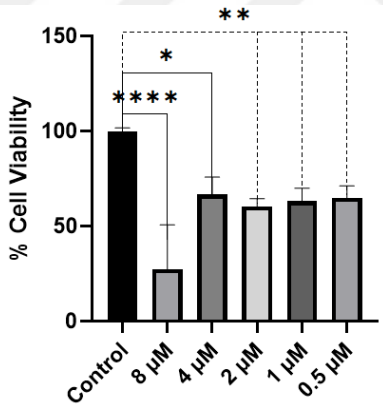

Figure 14: Cell viability data after 72 hours of incubation to determine the optimum $A\beta_{1-42}$ peptide concentration in a 2D AD model

3.2.2 3D Cell Viability

In the 3D monoculture AD model, the optimum $A\beta_{1-42}$ concentration was found to be 20 µM after 48 hours of incubation. In the 3D AD model, no statistically significant change in cell viability was observed after 24 hours of incubation with $A\beta_{1-42}$ peptide.

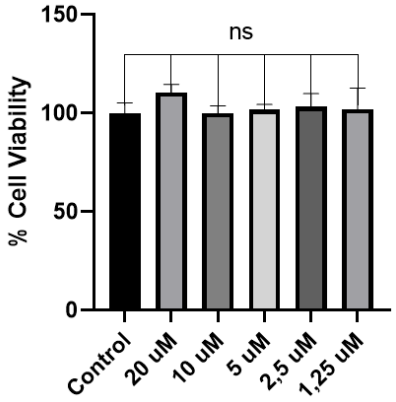

Figure 15: Cell viability data after 24-hour incubation to determine the optimum $A\beta_{1-42}$ peptide concentration in a 3D monoculture AD model

In contrast to 24 hours, after 48 hours, a significant decrease (*$p \leq 0.05$) occurred at the initial $A\beta_{1-42}$ concentration of 20 µM in the 3D AD model compared to the other concentrations. The optimal amount of $A\beta_{1-42}$ in the 3D AD model was determined to be 20 µM. Cell viability results are shown below in Figure 16.

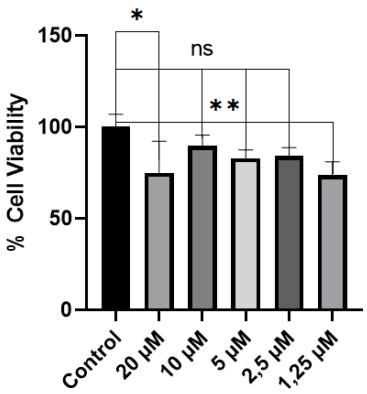

Figure 16: Cell viability data after 48 hours of incubation to determine the optimum $A\beta_{1-42}$ peptide concentration in a 3D AD model

3.2.3 2D Co-Culture Cell Viability

In the model optimized by co-culture of the 2D AD model developed with SHSY5Y and N9 cells and added 1 mg/mL LPS and 10 µM $A\beta_{1-42}$ peptide as an initial

concentration, a decrease in cell viability occurred at 10 µM $A\beta_{1-42}$. Details are shown in Figure 17.

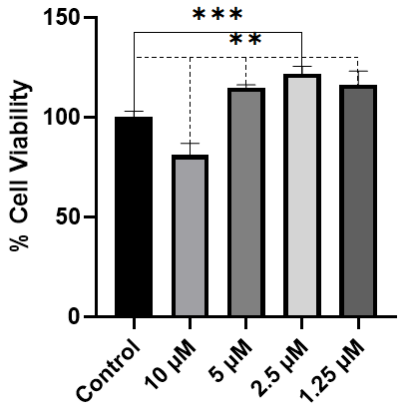

Figure 17: Cell viability data after 48 hours of incubation to determine the optimal $A\beta_{1-42}$ peptide concentration in the 2D Co-culture AD model

3.2.4 3D Co-Culture Cell Viability

To determine the optimal concentration of $A\beta_{1-42}$ peptide, a 3D AD model consisting of SHSY5Y and N9 cells was incubated with 20 µM and diluted concentrations of $A\beta_{1-42}$ peptide and 1 mg/mL LPS for 48 hours. In Figure 18, cell viability results showed that 20 µM $A\beta_{1-42}$ peptide increased cell viability after 48 hours, but this increase was not statistically significant compared to the control group.

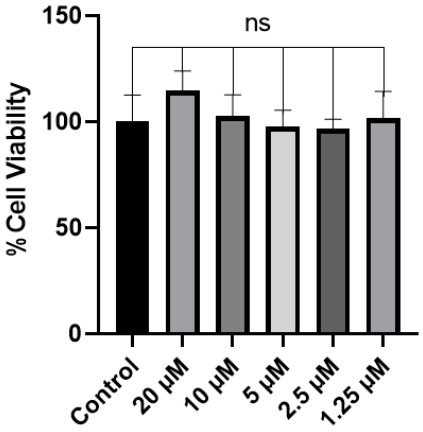

Figure 18: Cell viability data after 48 hours of incubation with 1 mg/mL LPS to determine the optimal $A\beta_{1-42}$ peptide concentration in the 3D Co-culture AD model

3.3 Quantitative Real Time Polymerase Chain Reaction (qRT-PCR)

3.3.1 qRT-PCR Results for 2D AD Model

To establish the Real Time PCR set, the total RNA concentration and A260/A280 ratio obtained from SHSY5Y cells are shown in Table 1. When the amount of total RNA obtained from cells in the 2D AD model was examined, the concentration in the control group was almost three times higher than in the AD model. RNA integrity and purity were assessed by spectrophotometry, and only samples with an A260/A280 ratio between 1.8 and 2.0 were used for RT-PCR.

Table 1: Concentrations and purities of RNAs obtained from control and 2D AH model groups

	A260/A280	**Concentration (ng/µL)**
Control	2,01	1378,10
2D AD Model	1,99	489,57

Changes in mRNA expression levels with *ADAM9, APP, BACE1, MAPT, ACHE, BDNF, CREB* and *βACT* primers were demonstrated by quantitative PCR and the results are given in Figure 19. When the genes expressed in the 2D AD model were examined, significant increases were observed in APP, *BACE1, and MAPT* expression levels, while no statistically significant changes were detected in *ACHE,* and *CREB*. Also, ADAM9 and BDNF genes expression levels statistically were decreased.

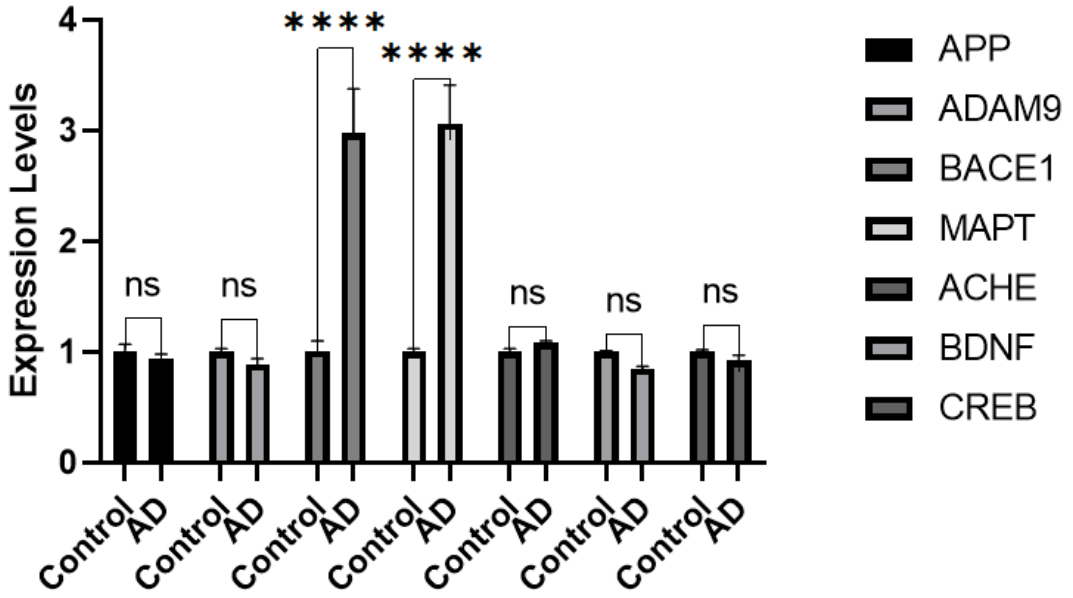

Figure 19: Relative *APP, ADAM9, BACE1, MAPT, ACHE, BDNF* and *CREB* genes expression levels in 2D AD and control groups

3.3.2 qRT-PCR Results for 3D AD Model

The concentration and purity of the isolated total RNAs were measured spectrophotometrically, and the results are presented in Table 2. In 3D AD model, spectrophotometric analysis (A260/A280) indicated that the samples were sufficiently pure for qRT-PCR. Total RNA concentration was higher in this group than the control group.

Table 2: Amount and purity of RNA obtained from the 3D AD model and control group

	A260/A280	**Concentration (ng/µL)**
Control	1,95	233,78
3D AD Model	1,97	394,00

The relative expression levels of genes are presented in Figure 20. According to qRT-PCR results, the genes with increased expression levels in the AD model compared to the control group were *BACE1, MAPT*, and *ACHE*, while *ADAM9, BDNF,* and *CREB genes* showed decreased expression. No significant difference was observed in *APP* gene expression level.

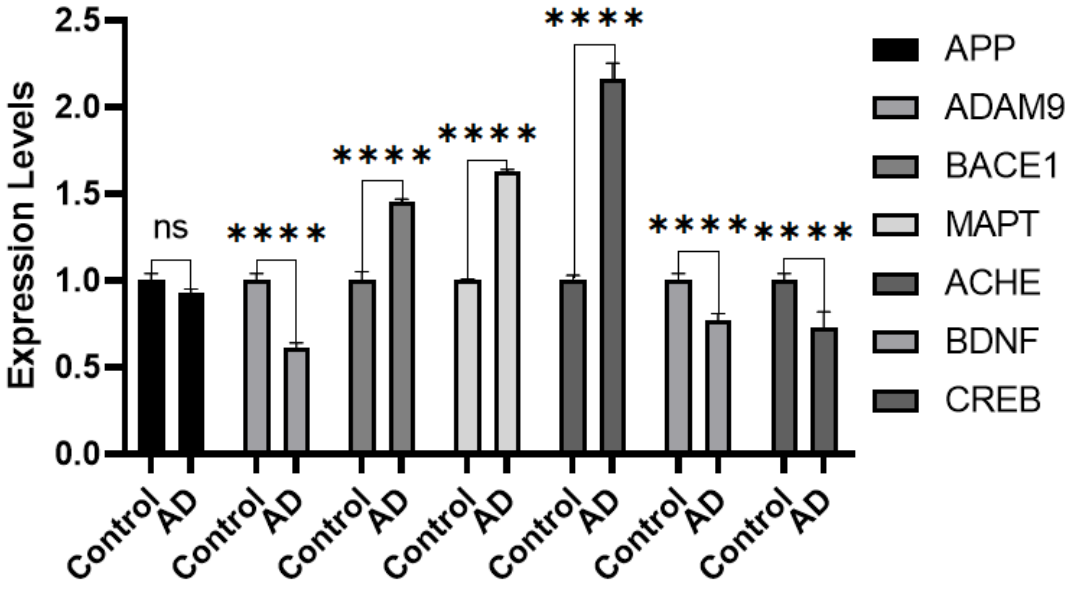

Figure 20: Relative *APP, ADAM9, BACE1, MAPT, ACHE, BDNF* and *CREB* expression levels of 3D AD and control groups

3.3.3 qRT-PCR Results for 2D Co-Culture AD Model

Results including RNA concentrations and A260/280 values are presented in Table 3. Spectrophotometric measurements showed that the isolated RNAs were of sufficient concentration and purity, and no contamination was detected according to the A260/280 ratio.

Table 3: Amount and purity of RNA obtained from the 2D co-culture AD model and control group

	A260/A280	**Concentration (ng/µL)**
2D Co-Culture Control	1,94	83,55
2D Co-Culture AD Model	1,74	29,59

Changes in mRNA expression levels with *ADAM9, APP, BACE1, MAPT, ACHE, BDNF,* and *CREB* primers were demonstrated by qRT-PCR and the results are given in Figure 21. qRT-PCR analysis demonstrated that, in the 2D co-culture AD model, expression levels of *APP, ADAM9, BACE1, ACHE, BDNF,* and *CREB* genes were significantly reduced compared with the control group. *MAPT* expression was not detectable in this model.

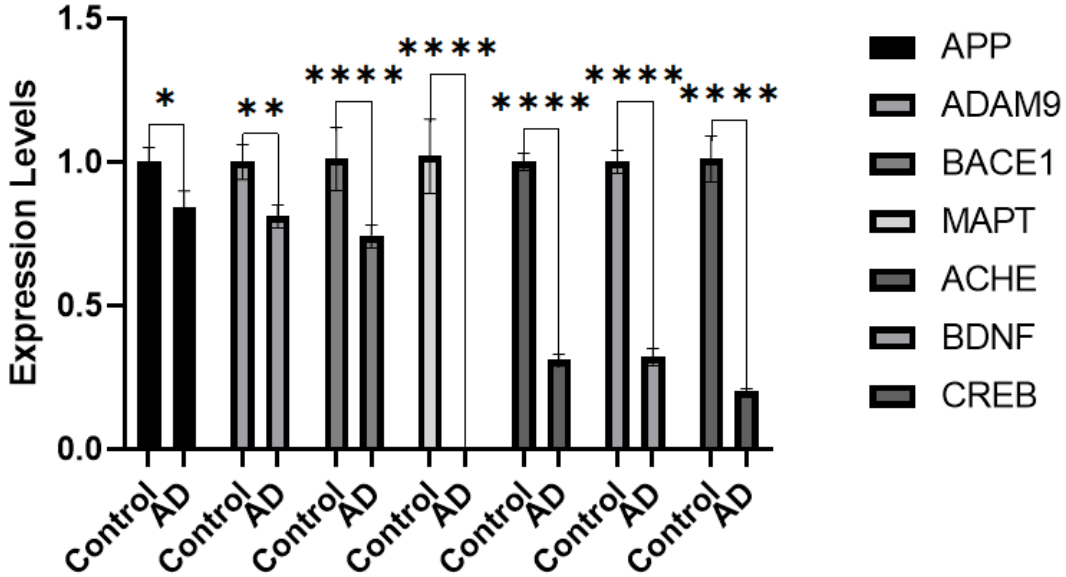

Figure 21: Relative *APP, ADAM9, BACE1, MAPT, ACHE, BDNF* and *CREB* expression levels of 2D co-culture AD and control groups

3.3.4 qRT-PCR Results for 3D Co-Culture AD Model

The quality of the nucleic acids was verified, and samples meeting the purity threshold were subjected to RT-PCR analysis. These outcomes are presented in Table 4.

Table 4: Amount and purity of RNA obtained from the 3D co-culture AD model and control group

	A260/A280	**Concentration (ng/µL)**
3D Co-Culture Control	1,97	83,55
3D Co-Culture AD Model	1,98	29,59

According to qRT-PCR analysis, in the 3D co-culture AD model, *APP, ADAM9,* and *BACE1* expression levels were significantly upregulated compared to the control group. Conversely, MAPT, BDNF and *CREB* were downregulated, while *ACHE* expression was present at low but measurable levels. The overall gene expression patterns are illustrated in Figure 22.

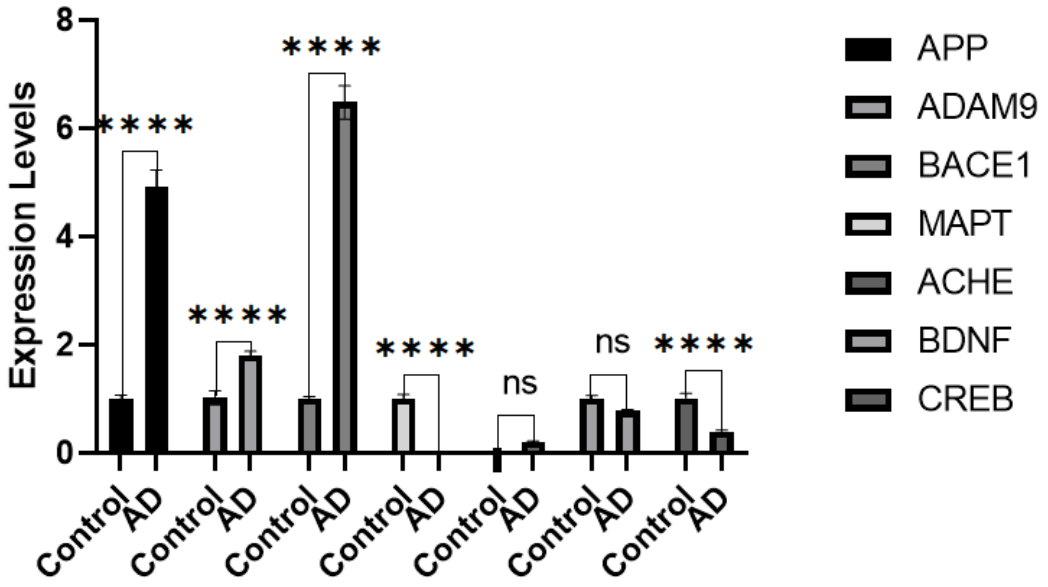

Figure 22: Relative *APP, ADAM9, BACE1, MAPT, ACHE, BDNF* and *CREB* expression levels of 3D co-culture AD and control groups

3.4 Bicinchoninic Acid Assay (BCA)

In BCA analysis, a graph was created to determine protein concentrations and unknown protein concentrations were calculated using the resulting equation. y=0.001x+0.1765 and R^2=0.996. The standard curve graph is shown in Figure 23.

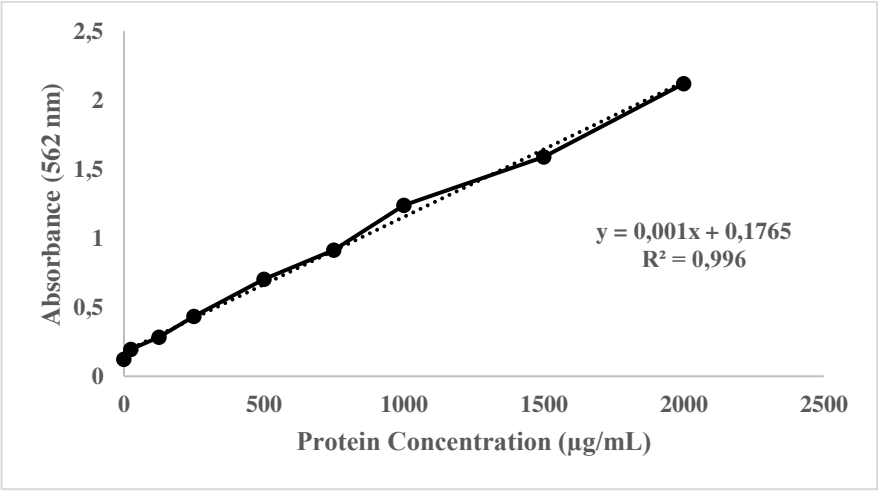

Figure 23: Standard curve used for BCA analysis

Protein values were measured spectrophotometrically at a wavelength of 562 nm and the values obtained are shown in the Table 5. Since the optimum $A\beta_{1-42}$ concentration could not be optimized in coculture AD models, the highest applied $A\beta_{1-42}$ concentration was used in the experiments.

Table 5: Protein values measured in the AD model and control group

	Control (mg/mL)	**AD Model (mg/mL)**
2D AD	0,85 ± 0,03	0,30 ± 0,08
3D AD	0,63 ±0,08	0,58 ±0,10
2D Co-culture AD	0,28 ± 0,05	0,19 ±0,04
3D Co-culture AD	0,50 ± 0,07	0,58 ± 0,07

3.5 Acetylcholinesterase (AchE) Activity

In AchE analysis, a standard curve is created for the unknown amount of AchE from absorbance values. Groups were analyzed using the One Sample t Test method. The equation obtained from the standard graph is $y = 0.001x + 0.1765$ and $R^2 = 0.996$. The created curve is shown in Figure 24.

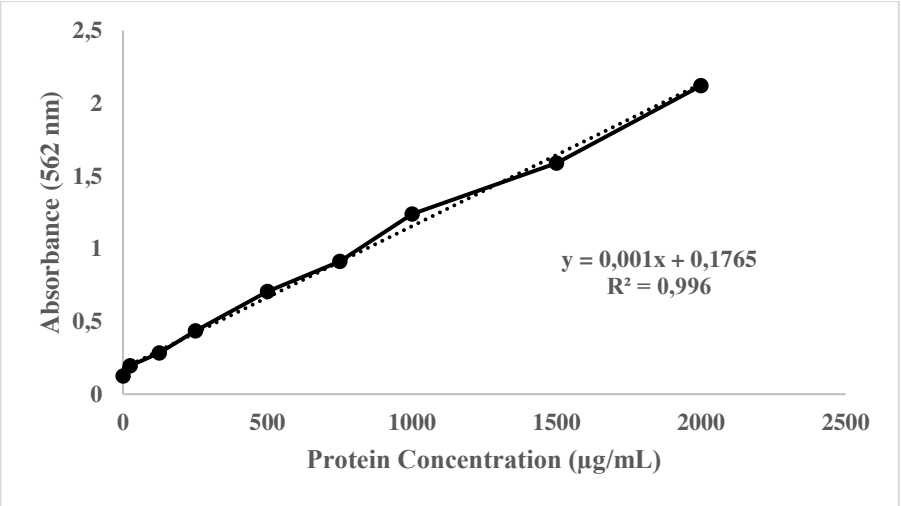

Figure 24: Standard Curve Used for Determination of AchE Activity

3.5.1 AchE Activity in 2D AD Model

The AchE activity of the 2D AD model created with SHSH5Y cells is evaluated in Figure 25. When the AchE activity of the AD model was evaluated, a statistically significant increase (***p≤0.001) was observed compared to the control group.

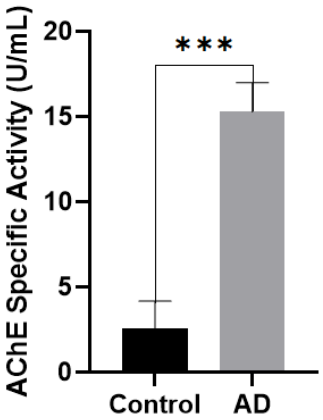

Figure 25: AchE Analysis in 2D AD Model

3.5.2 AchE Activity in 3D AD Model

The AchE Specific Activity results of the 3D AD model created with SHSY5Y cells are shown in Figure 26. A statistically significant increase (*p≤0.05) in AchE specific activity was observed in the AD model compared to the control group.

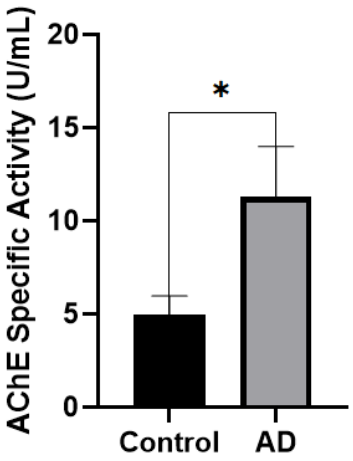

Figure 26: AchE Analysis in 3D AD Model

3.5.3 AchE Activity in 2D Co-Culture AD Model

The results of AchE specific activity in the 2D coculture AD model created with N9 and SHSY5Y cells are shown in Figure 27. Although there was no statistically significant difference in the amount of AchE specific activity in the AD model compared to the control group, an increase was observed.

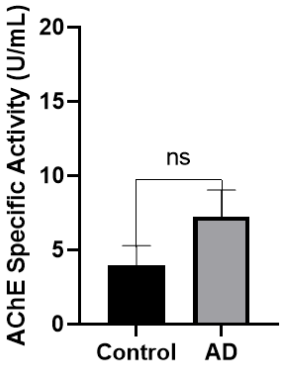

Figure 27: AchE Analysis in 2D Coculture AD Model

3.5.4 AchE Activity in 3D Co-Culture AD Model

The results of AchE specific activity in the 3D coculture AD model created with N9 and SHSY5Y cells are shown in Figure 28. When the AchE specific activity was compared, the AchE value of the control group was higher and no statistically significant difference was obtained between them.

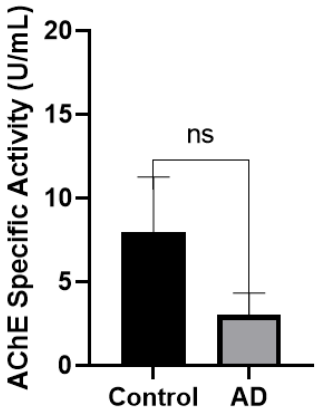

Figure 28: AchE Analysis in 3D Coculture AD Model

3.6 pMAPT/pTau Assay

The standard curve created to calculate the human pMAPT/pTau concentration obtained from the samples is given below. Also, results were analyzed using the One Sample t Test method. The curve equation is y=0.0008x+0.06638. The R^2 value was found to be 0.9996.

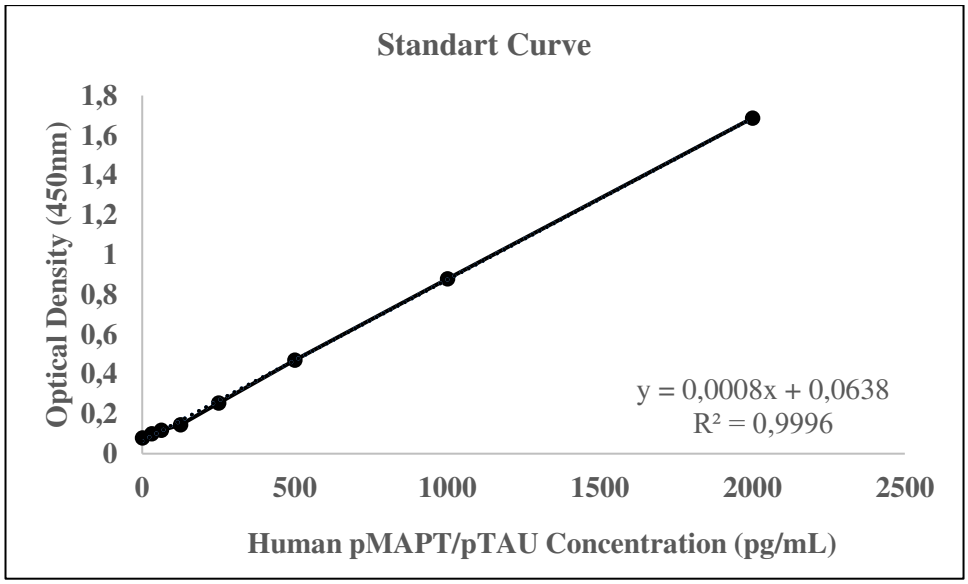

Figure 29. Standard curve graph created to calculate human pMAPT/pTAU amount

3.6.1 pMAPT/pTAU Analysis in 2D AD Model

The pMAPT/TAU results of the AD model created with SHSY5Y cells are shown in Figure 30. When the amount of pMAPT/TAU in the control group and the AD model was compared, a statistically significant increase occurred in the AD model (****p≤0.0001).

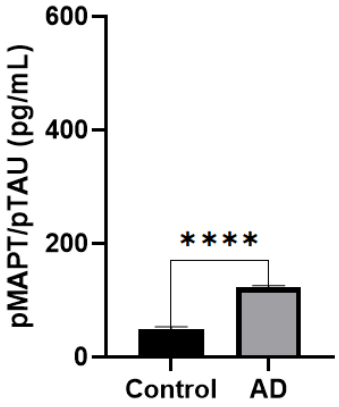

Figure 30: pMAP/TAU Analysis in 2D AD Model

3.6.2 pMAPT/pTAU Analysis in 3D AD Model

The pMAP/TAU results of the 3D AD model created with SHSY5Y cells are shown in Figure 31. According to the results, the amount of pMAP/TAU increased in the AD model compared to the control group (*p≤0.05).

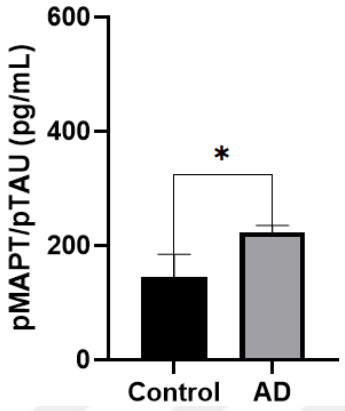

Figure 31: pMAP/TAU Analysis in 3D AD Model

3.6.3 pMAPT/pTAU Analysis in 2D Co-Culture Model

The pMAPT/pTAU results in the coculture AD 2D model created with N9 and SHSY5Y cells are shown in Figure 32. The amount of pMAPT/pTAU showed a statistically significant increase (*p≤0.05) in the control group compared to the AD model group.

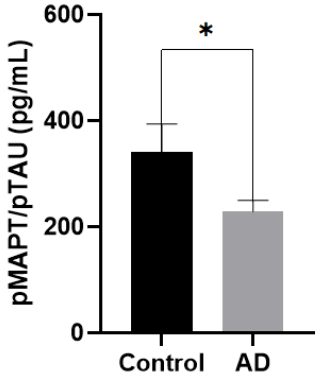

Figure 32: pMAPT/pTAU Analysis in 2D Co-Culture AD Model

3.6.4 pMAPT/pTAU Analysis in 3D Co-Culture Model

The pMAPT/pTAU results in the coculture AD 3D model created with N9 and SHSY5Y cells are shown in Figure 33. The amount of pMAPT/pTAU was higher in the control group than in the AD model, but not significant difference was observed between them.

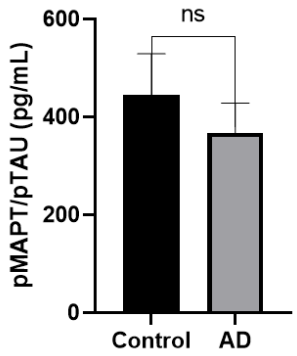

Figure 33: pMAPT/pTAU Analysis in 3D Coculture AD Model

SECTION FOUR

4. DISCUSSION

Cell viability results showed that the $A\beta_{1-42}$ concentration that made a significant difference in the 2D AD model was 8 µM after 48 h of incubation, as shown in Figure 13. However, because cell viability continued to decrease dramatically, the $A\beta_{1-42}$ concentration used in the development of the AD model was 4 µM after 48 h of incubation. In designing the 3D AD model, the optimum $A\beta_{1-42}$ concentration for 48 h was determined as 20 µM, as shown in Figure 16. As presented in Figure 18, $A\beta_{1-42}$ administration did not cause a significant change in cell viability in the co-culture model. However, while a decrease in cell viability was expected at 48 hours, as in the 2D mono-culture AH model, an increase in cell viability was observed in the 2D co-culture AH model. It is thought that this situation may have occurred due to the proliferation of microglia activated by proinflammatory stimuli (LPS). (Zhang et al., 2024).

In the microscope images of the 2D AD monoculture and co-culture models shown in Figures 5 and 10. When the images were examined, it was seen that cell morphology in AD models changed compared to the control groups and cells demonstrated disrupted integrity. These results clearly demonstrate that amyloid beta peptide in the culture medium exhibits toxicity (Wiles et al., 2017). In the 3D co-culture AD model images shown in Figure 10, it is noteworthy that the cells form bulky structures instead of the typical microtissue form, and irregular boundaries are observed even in the control group. Bassil and colleagues (2021) reported that co-culturing mouse and human cells weakened cell-to-cell interactions. Similarly, this study also involved co-culturing cells of different origins (mouse and human), which may have led to poor cell-to-cell interactions. Possible reasons for this could include differences in cell metabolic rates or changes in the culture medium (Vis et al., 2020).

AD model was established in both 2D and 3D monoculture systems, and differences in disease-related gene expression were detected. As shown in Figure 19, in the 2D AD monoculture model compared to the control *BACE1, APP, MAPT* gene expressions were significantly upregulated, while *ADAM9 and BDNF* gene expression

was downregulated. *ACHE,* and *CREB* expression was not significant. However, when the ACHE levels measured by ELISA at the protein level in Figure 25 were examined, an increase is observed in the AD model. This suggests that *ACHE* mRNA may have been degraded within the cell but was captured by the ELISA because translation occurs, and the protein is released outside the cell. Therefore, the reason for the lack of *ACHE* gene expression observed in qRT-PCR may be that the mRNA is degraded within the cell before being translated into protein (Shaltiel et al., 2012). *BDNF,* a key regulator of neuronal survival and plasticity, was decreased in the AD model, confirming its role in synaptic dysfunction and cognitive decline (Baghi et al., 2021). *CREB,* a transcription factor activated by *BDNF* signaling, also showed reduced expression, further supporting impaired neuronal survival pathways (Sheng et al., 2012; Sohn et al., 2021).

In the 3D AD monoculture model, which shown in Figure 20, APP levels did not show a significant change, whereas *ADAM9, BDNF, and CREB* were decreased, and *BACE1, MAPT*, and *ACHE* genes expression were markedly increased. Reduced *APP* expression in the 3D system may be explained by $A\beta_{1\text{-}42}$ supplementation suppressing *APP* transcription (Martinsson et al., 2022), hypoxic stress within the 3D environment, or the fact that 3D culture more closely mimics *in vivo APP* regulation compared to 2D (Whitehouse et al., 2025; Fang et al., 2024).

ADAM9 downregulation in both models (2D and 3D monoculture) indicates enhanced *APP* cleavage by β-secretase, promoting Aβ accumulation (Moss et al., 2011). The observed increase in *BACE1* supports literature findings that β-secretase activity is elevated under oxidative stress and inflammation in AD pathology (Cervellati et al., 2019; Baek et al., 2025). *MAPT* upregulation in both systems suggests tau hyperphosphorylation and tangle formation, supporting AD establishment (Gultekin et al., 2024; Zheng et al., 2023). Elevated *ACHE* levels confirm cholinergic dysfunction and decreased acetylcholine availability (Deenathayalan & Brindha et al., 2023; Sivaraman et al., 2022). Together, these results indicate that the 3D monoculture AD model reflects AD pathology more accurately than the 2D model (Ko et al., 2022).

In the 2D co-culture AD model shown in Figure 21, *APP* expression was significantly decreased in the AD group compared to the control, although an increase would generally be expected in Alzheimer's pathology due to its role as the precursor

of Aβ peptides. This reduction may reflect transcriptional feedback inhibition caused by Aβ accumulation or inflammatory regulation mediated by microglia (Park, et al., 2024). *ADAM9* expression was also reduced, which is consistent with the shift of *APP* processing from the α-secretase to the β-secretase pathway (Wang, et al., 2024). In contrast, *BACE1* expression was markedly increased, supporting the enhanced amyloidogenic processing observed in AD (Andrew, et al., 2017). *MAPT* levels didn't expressed in the AD model. Importantly, both *ACHE,* BDNF and *CREB* expression were decreased. These results may highlight that microglial activation in the 2D culture contributes to anti-inflammatory signaling thereby supporting neuronal survival and synaptic plasticity (Feng, et al., 2020).

In the 3D co-culture AD model, which shown in Figure 22, a different pattern was observed. *APP* expression was strongly increased in the AD group compared to controls, suggesting that the combined effects of hypoxia and microglial-derived inflammation in the 3D environment more profoundly suppress *APP* transcription (Kauppinen et al., 2011). *ADAM9* expression was elevated, whereas *BACE1* showed robust increases, confirming the activation of amyloid and tau pathologies. Interestingly, *ACHE and BDNF* expression did not show a significant change, whereas *CREB* expression was markedly reduced. *BDNF* transcription is relatively preserved in the 3D system. Similar to the work of Yin et al., our findings suggest that this model can also exhibit proinflammatory responses, as observed in the 2D co-culture model. These results are consistent with data reported in the literature (Yin, et al., 2020).

Taken together, in the co-culture models, microglia appear to play a protective role. Although several genes such as *BACE1, MAPT, APP* reflect AD pathology, further confirmation is required by examining inflammatory mediators such as TNF-α and TGF-β. On the other hand, in the monoculture models (2D and 3D), the consistent upregulation of AD-related genes supports that an AD model has been successfully established.

When BCA results were evaluated, the 3D AD model generated with SHSY5Y cells had the highest protein concentration. Interestingly, although viability was high in the 2D co-culture AD model, the resulting protein concentration was significantly lower than in the 2D AD model. There is a complex relationship between protein concentration and viability. High protein concentrations can lead to protein

misfolding, which can lead to apoptosis in cells, or activate different signaling pathways within the cell, enabling survival (Akter et al., 2019). Therefore, particularly in 2D AD modeling, a low protein concentration despite high viability can indicate misfolding or degraded protein levels.

When AchE levels were examined which is shown in Figure 25 and Figure 26, monoculture AD model, an increase in AchE levels was observed in both the 2D and 3D models, as expected. However, the results in the cocultured AD model which found in the Figure 27 and Figure 28 were slightly different. An increase in AchE levels was observed in the 2D cocultured AD model, but this increase was not statistically significant. In the 3D model, the control group had higher AchE levels. This may be because the 3D *in vitro* environment better mimics the real AD microenvironment (Tao et al., 2022). Neuronal responses from SHSYS5Y cells may have been suppressed in the presence of LPS (Mátis et al., 2017). This explains the lower than expected AchE release in both the 2D and 3D constructs. Another reason may be that activated microglia due to the proinflammatory response due to the presence of $A\beta_{1-42}$ may activate the P2Y6 and P2X7 signaling pathways, which are responsible for the regulation of proinflammatory responses (Ngamjariyawat et al., 2013).

As shown in Figures 30 and 31, pMAPT/TAU levels in SH-SY5Y cells were significantly different in pMAPT/pTAU compared to the control, consistent with AD.This is because the amount of pTAU, a pathological marker of AD, increases, leading to NFTs. The presence of $A\beta_{1-42}$ also expressed genes characteristic of AD at the cellular level. However, the most striking results for pMAPT/pTAU were obtained in the 2D and 3D AD models generated with cocultured N9 and SHSY5Y cells shown in Figure 32 and Figure 33. In the Figure 32, 2D AD model, pTAU levels were higher in the $A\beta_{1-42}$ and LPS-free group than in the LPS-containing group. This may be due to several factors. First, it is suggested that N9 and SHSY5Y cells are of different origins (Vatter & Brinton, 2014). The interaction between Aβ and tau depends on the microenvironment. The regulatory mechanisms of tau protein may be inactivated in the presence of LPS (Rajendrakumar et al., 2024). For a similar reason, the addition of N9 microglia to the coculture medium may have hindered the measurement of pTau levels due to the cytokines they secrete as a result of the immune response. Conversely, the proinflammatory response may have increased the ability to prevent tau from

becoming hyperphosphorylated, thus reducing its hyperphosphorylation (Feng et al., 2019).

The findings obtained from the 3D co-culture Alzheimer's disease model do not overlap with the results obtained from the 3D monoculture model and even reveal opposite responses. There are several possible explanations for this: First, SHSY5Y cells are human-derived neuroblastoma cells, while N9 cells are mouse-derived microglia. The use of human and mouse cells in this study is linked to the existence of evolutionarily conserved biological pathways across species, as these two species share orthologous genes. In *in vivo* experiments, mouse models capable of mimicking Aβ protein accumulation through mutations in the *APP* gene are widely used, allowing for the convenient modeling of Alzheimer's disease pathology due to the presence of orthologs (Yokoyama et al., 2022). But in these research coculture of cells from different species may not produce the expected cytokine responses or metabolic activities. Cell-cell interactions or signals that activate pathways may come from different origins, which may have caused the signals not to be transmitted (Vatter & Brinton, 2014). Therefore, AD may have progressed in this model due to degeneration of SHSY5Y cells. Third, in the presence of LPS, microglia have the ability to kill healthy cells. The additional presence of different cell lines and the human origin of SHSY5Y may have led to its perception as an additional pathogen (Dai et al., 2015).

In summary, the AD model generated in the presence of SHSYSY and $A\beta_{1-42}$ exhibited the expected AD markers, while the AD model in coculture did not. This is primarily due to the different origins of the cocultured cells (Vatter & Brinton, 2014). Another reason is that creating a coculture AD model using the 3D Petri Dish method may not be appropriate. An alternative to this method is to create an AD model using an insert. In this case, microglia activated in the presence of LPS and $A\beta_{1-42}$will not phagocytose the SHSY5Y cells, providing the necessary signals and cytokines, thus eliminating a decrease in cell viability and resulting in more accurate results. This will allow for a more controlled microenvironment (Beca et al., 2019). However, this method can also yield more accurate results using human derived HMC3 microglia.

Instead of microglia, which also cause an increase in cell numbers as a proinflammatory response, astragalus cells, which change cell morphology when activated, may be suitable for studying the immune system and AD disease (Ontiveros-

Ángel et al., 2024). Another reason is that, especially in the 3D co-culture AD model, an anti-inflammatory response was expected in this model. However, considering that the 3D model better mimics the real microenvironment, the AD model may exhibit an anti-inflammatory response rather than a pro-inflammatory response. This may explain the decreased levels of cell viability, AchE and pTau in the 3D coculture AD model compared to other groups (Jang et al., 2020; Pišlar, et al., 2021).

SECTION FIVE

5. CONCLUSION & RECOMMENDATIONS

In this study, the Alzheimer's disease model created by using the SHSY5Y cell line as a monoculture and adding the $A\beta_{1-42}$ peptide, as well as 2D and 3D models in which SHSY5Y and N9 cell lines were co-cultured and LPS was added to ensure microglial activation in addition to the $A\beta_{1-42}$ peptide, were evaluated in a multifaceted manner. While a significant decrease in cell viability was observed after 48 hours of incubation following application of 8 μM $A\beta_{1-42}$ in the 2D model, this decrease became evident only at a concentration of 20 μM in the 3D model. In coculture models, application of 10 μM $A\beta_{1-42}$ resulted in an increase in viability. However, in general, the optimum concentration of AD models created solely with SHSY5Y have been confirmed to be successful through quantitative analyses. But coculture AD models created with N9 and SHSY5Y cells did not yield results as successful as those using a single cell line. This, in turn, demonstrates that the immune system influences AD pathology. Therefore, anti-inflammatory tests with TNF-β or pro-inflammatory tests with TNF-α could illuminate the model's characterization. The 3D Petri Dish method may not be suitable for coculture. To understand this, different 3D *in vitro* methods, such as inserts, could be used. To investigate the effects of AD on the immune system, astrocytes, which are members of the adaptive immune system, can be used instead of microglia because they change morphology when activated. Peptide in the 3D environment was determined to be 20 μM. Similarly, pMAPT/pTAU levels increased significantly in 2D and 3D SHSY5Y models, while a decrease was observed in coculture models compared to the control group, but this difference was not statistically significant. Overall, these findings demonstrate the effectiveness of AD models developed with SHSY5Y and N9 cells on pathological markers and indicate that cellular responses may vary in different models.

2D and 3D AD models developed with SHSY5Y have been confirmed to be successful through quantitative analyses. While the co-culture AD models with N9 and SHSY5Y cells did not mirror the monoculture AD model outcomes, they provided additional insights into cell–cell interactions relevant to Alzheimer’s disease. This, in

turn, demonstrates that the immune system influences AD pathology. In the co-culture AD models may have pro-inflammatory response. Therefore, anti-inflammatory tests with TNF-β or pro-inflammatory test TNF-α with could illuminate the model's characterization. The 3D Petri Dish method may have limitations when applied to co-culture systems. To understand this, different 3D *in vitro* methods, such as inserts, could be used. To investigate the effects of AD on the immune system, astrocytes, can be used instead of microglia because they change morphology when activated.

5. REFERENCES

Abdul Manap, A. S., Almadodi, R., Sultana, S., Sebastian, M. G., Kavani, K. S., Lyenouq, V. E., & Shankar, A. (2024). Alzheimer's disease: A review on the current trends of the effective diagnosis and therapeutics. *Frontiers in Aging Neuroscience*, *16*, 1429211.

Agarwal, S., Saha, S., Balla, V. K., Pal, A., Barui, A., & Bodhak, S. (2020). Current developments in 3D bioprinting for tissue and organ regeneration–a review. *Frontiers in Mechanical Engineering*, *6*, 589171.

Agholme, L., Lindström, T., Kågedal, K., Marcusson, J., & Hallbeck, M. (2010). An in vitro model for neuroscience: differentiation of SH-SY5Y cells into cells with morphological and biochemical characteristics of mature neurons. *Journal of Alzheimer's disease*, *20*(4), 1069-1082.

Akter, S., Addepalli, R., Netzel, M. E., Tinggi, U., Fletcher, M. T., Sultanbawa, Y., & Osborne, S. A. (2019). Antioxidant-rich extracts of Terminalia ferdinandiana interfere with estimation of cell viability. *Antioxidants*, *8*(6), 191.

Al-Dulimi, Z., Wallis, M., Tan, D. K., Maniruzzaman, M., & Nokhodchi, A. (2021). 3D printing technology as innovative solutions for biomedical applications. *Drug Discovery Today*, *26*(2), 360-383.

Andrew, R. J., Fernandez, C. G., Stanley, M., Jiang, H., Nguyen, P., Rice, R. C., ... & Thinakaran, G. (2017). Lack of BACE1 S-palmitoylation reduces amyloid burden and mitigates memory deficits in transgenic mouse models of Alzheimer's disease. *Proceedings of the National Academy of Sciences*, *114*(45), E9665-E9674.

Baek, S. H., Hong, S., Kim, E., Park, S., Lee, M., Park, J., ... & Jo, D. G. (2025). A novel RAGE modulator induces soluble RAGE to reduce BACE1 expression in Alzheimer's disease. *Advanced Science*, *12*(8), 2407812.

Baghi, M., Yadegari, E., Rostamian Delavar, M., Peymani, M., Ganjalikhani-Hakemi, M., Salari, M., ... & Ghaedi, K. (2021). MiR-193b deregulation is associated with Parkinson's disease. *Journal of Cellular and Molecular Medicine*, *25*(13), 6348-6360.

Bassil, R., Shields, K., Granger, K., Zein, I., Ng, S., & Chih, B. (2021). Improved modeling of human AD with an automated culturing platform for iPSC neurons, astrocytes and microglia. *Nature Communications*, *12*(1), 5220.

Beca, B. M., Sun, Y., Wong, E., Moraes, C., & Simmons, C. A. (2019). Dynamic bioreactors with integrated microfabricated devices for mechanobiological screening. *Tissue Engineering Part C: Methods*, *25*(10), 581-592.

Benam, K. H., Dauth, S., Hassell, B., Herland, A., Jain, A., Jang, K. J., ... & Ingber, D. E. (2015). Engineered in vitro disease models. *Annual Review of Pathology: Mechanisms of Disease*, *10*(1), 195-262.

Benmeridja, L., De Moor, L., De Maere, E., Vanlauwe, F., Ryx, M., Tytgat, L., ... & Declercq, H. (2020). High-throughput fabrication of vascularized adipose microtissues for 3D bioprinting. *Journal of Tissue Engineering and Regenerative Medicine*, *14*(6), 840-854.

Bird, T. D. (2008). Genetic aspects of Alzheimer disease. *Genetics in medicine*, *10*(4), 231-239.

Bu, G. (2009). Apolipoprotein E and its receptors in Alzheimer's disease: pathways, pathogenesis and therapy. *Nature Reviews Neuroscience*, *10*(5), 333-344.

Caccamo, A., Maldonado, M. A., Bokov, A. F., Majumder, S., & Oddo, S. (2010). CBP gene transfer increases BDNF levels and ameliorates learning and memory deficits in a mouse model of Alzheimer's disease. *Proceedings of the National Academy of Sciences*, *107*(52), 22687-22692.

Casaletto, K., Ramos-Miguel, A., VandeBunte, A., Memel, M., Buchman, A., Bennett, D., & Honer, W. (2022). Late-life physical activity relates to brain tissue synaptic integrity markers in older adults. *Alzheimer's & Dementia*, *18*(11), 2023-2035.

Colonna, M., & Butovsky, O. (2017). Microglia function in the central nervous system during health and neurodegeneration. *Annual review of immunology*, *35*, 441-468.

Cerejeira, J., Lagarto, L., & Mukaetova-Ladinska, E. B. (2012). Behavioral and psychological symptoms of dementia. *Frontiers in neurology*, *3*, 73.

Cervellati, C., Trentini, A., Rosta, V., Passaro, A., Bosi, C., Sanz, J. M., ... & Zuliani, G. (2020). Serum beta-secretase 1 (BACE1) activity as candidate biomarker for late-onset Alzheimer's disease. *GeroScience*, *42*(1), 159-167.

Chaudhary, S., Kaushik, M., Ahmed, S., Kukreti, R., & Kukreti, S. (2018). Structural switch from hairpin to duplex/antiparallel G-quadruplex at single-nucleotide polymorphism (SNP) site of human apolipoprotein E (APOE) gene coding region. *ACS omega, 3(3),* 3173-3182.

Chen, Y., Huang, X., Zhang, Y. W., Rockenstein, E., Bu, G., Golde, T. E., ... & Xu, H. (2012). Alzheimer's β-secretase (BACE1) regulates the cAMP/PKA/CREB pathway independently of β-amyloid. *Journal of Neuroscience*, *32*(33), 11390-11395.

Chen, Z. R., Huang, J. B., Yang, S. L., & Hong, F. F. (2022). Role of cholinergic signaling in Alzheimer's disease. *Molecules*, *27*(6), 1816.

Collins, S. D., Yuen, G., Tu, T., Budzinska, M. A., Spring, K., Bryant, K., & Shackel, N. A. (2019). In vitro models of the liver: disease modeling, drug discovery and clinical applications. *Exon Publications*, 47-67.

Çınar, R. (2022). Depletion of glutathione induced apoptosis and oxidative stress via the activation of TRPM2 channels in the microglia cells with Alzheimer'disease model. *Journal of Cellular Neuroscience and Oxidative Stress*, *14*(1), 1063-1073.

Dai, D. L., Li, M., & Lee, E. B. (2023). Human Alzheimer's disease reactive astrocytes exhibit a loss of homeostastic gene expression. *Acta neuropathologica communications*, *11*(1), 127.

Dai, M. H., Zheng, H., Zeng, L. D., & Zhang, Y. (2017). The genes associated with early-onset Alzheimer's disease. *Oncotarget*, *9*(19), 15132.

Dai, D. L., Li, M., & Lee, E. B. (2023). Human Alzheimer's disease reactive astrocytes exhibit a loss of homeostastic gene expression. *Acta neuropathologica communications*, *11*(1), 127.

Dai, X. J., Li, N., Yu, L., Chen, Z. Y., Hua, R., Qin, X., & Zhang, Y. M. (2015). Activation of BV2 microglia by lipopolysaccharide triggers an inflammatory reaction in PC12 cell apoptosis through a toll-like receptor 4-dependent pathway. *Cell Stress and Chaperones*, *20*(2), 321-331.

Deenathayalan, U., & Brindha, D. (2023). Arbutin aids in the recovery of dyskinesia in Alzheimer's zebrafish by decreasing the function of acetylcholinesterase. *Arbutin aids in the recovery of dyskinesia in Alzheimer's zebrafish by decreasing the function of acetylcholinesterase*, *18*(4).

de Medeiros, L. M., De Bastiani, M. A., Rico, E. P., Schonhofen, P., Pfaffenseller, B., Wollenhaupt-Aguiar, B., ... & Klamt, F. (2019). Cholinergic differentiation of human neuroblastoma SH-SY5Y cell line and its potential use as an in vitro model for Alzheimer's disease studies. *Molecular neurobiology*, *56*(11), 7355-7367.

Diniz, D. G., Bento-Torres, J., da Costa, V. O., Carvalho, J. P. R., Tomás, A. M., Galdino de Oliveira, T. C., ... & Picanço Diniz, C. W. (2024). The hidden dangers of sedentary living: insights into molecular, cellular, and systemic mechanisms. *International Journal of Molecular Sciences*, *25*(19), 10757.

Dodurga, Y., Gundogdu, G., Koc, T., Yonguc, G. N., Kucukatay, V., & Satiroglu-Tufan, N. L. (2013). Expressions of URG4/URGCP, cyclin D1, Bcl-2, and Bax genes in retinoic acid treated SH-SY5Y human neuroblastoma cells. *Contemporary Oncology/Współczesna Onkologia*, *17*(4), 346-349.

Dogan, A. A. (2017). *Üç boyutlu (3B) in vitro Parkinson hastalığı modelleri oluşturulması ve oluşturulan modellerin karakterizasyonu* (Yüksek lisans tezi). Ege Üniversitesi, Fen Bilimleri Enstitüsü, İzmir

Doğan, A. A., Taşdemir, Ş., & Ürkmez, A. Ş. (2016). SH-SY5Y VE SK-N-AS HÜCRE HATLARININ MİKRODOKU OLUŞTURMA KAPASİTELERİNİN KARŞILAŞTIRILMASI. *Dokuz Eylül Üniversitesi Mühendislik Fakültesi Fen ve Mühendislik Dergisi*, *18*(52), 40-48.

Dousti, M., Parsa, S., Sani, F., Bagherzadeh, E., Zamanzadeh, Z., Dara, M., ... & Azarpira, N. (2024). Enhancing bone regeneration: Unleashing the potential of

magnetic nanoparticles in a microtissue model. *Journal of Cellular and Molecular Medicine*, *28*(17), e70040.

Duran, R., Pancur, S., & Bahadori, F. (2022). The Effect of Type 2 Diabetes Mellitus on the Development of Alzheimer's Disease and Its Molecular Mechanism.

Eskandari-Sedighi, G., & Blurton-Jones, M. (2023). Microglial APOE4: more is less and less is more. *Molecular Neurodegeneration*, *18*(1), 99.

Farooq, R., Jawad, U., Khan, I., Zia-ur-Rehman, M., Irfan, M., & Ullah, S. (2022). A cross-sectional study on behavioral manifestation in alzheimer's disease patients and their association with cognitive impairment. *PJMHS*, *16(2)*, 952-955.

Fang, J., Singh, S., Wells, B., Wu, Q., Jin, H., Janke, L. J., ... & Yang, J. (2025). The context-dependent epigenetic and organogenesis programs determine 3D vs. 2D cellular fitness of MYC-driven murine liver cancer cells. *eLife*, *14*, RP101299.

Farrimond, L. E., Roberts, E., & McShane, R. (2012). Memantine and cholinesterase inhibitor combination therapy for Alzheimer's disease: a systematic review. *BMJ open*, *2*(3), e000917.

Feng, T., Yamashita, T., Shang, J., Shi, X., Nakano, Y., Morihara, R., ... & Abe, K. (2019). Clinical and pathological benefits of edaravone for Alzheimer's disease with chronic cerebral hypoperfusion in a novel mouse model. *Journal of Alzheimer's Disease*, *71*(1), 327-339.

Feng, Q., Luo, Y., Zhang, X. N., Yang, X. F., Hong, X. Y., Sun, D. S., ... & Wang, J. Z. (2020). MAPT/Tau accumulation represses autophagy flux by disrupting IST1-regulated ESCRT-III complex formation: a vicious cycle in Alzheimer neurodegeneration. *Autophagy*, *16*(4), 641-658.

Foglietta F, Serpe L, Canaparo R. (2021). The effective combination between 3D cancer models and stimuli-responsive nanoscale drug delivery systems. *Cells, 10(12),* 3295.

Forster, J. I., Köglsberger, S., Trefois, C., Boyd, O., Baumuratov, A. S., Buck, L., ... & Antony, P. M. A. (2016). Characterization of differentiated SH-SY5Y as

neuronal screening model reveals increased oxidative vulnerability. *Journal of biomolecular screening*, *21*(5), 496-509.

Franco, R., & Cedazo-Minguez, A. (2014). Successful therapies for Alzheimer's disease: why so many in animal models and none in humans?. *Frontiers in pharmacology*, *5*, 146.

Gajendra, K., Pratap, G. K., Poornima, D. V., Shantaram, M., & Ranjita, G. (2024). Natural acetylcholinesterase inhibitors: a multi-targeted therapeutic potential in Alzheimer's disease. *European Journal of Medicinal Chemistry Reports*, *11*, 100154.

García-Ayllón, M. S., Small, D. H., Avila, J., & Sáez-Valero, J. (2011). Revisiting the role of acetylcholinesterase in Alzheimer's disease: cross-talk with P-tau and β-amyloid. *Frontiers in molecular neuroscience*, *4*, 22.

Gogniat, M. A., Khan, O. A., Li, J., Park, C., Hudson Robb, W., Zhang, P., ... & Jefferson, A. L. (2025). Increased sedentary behavior is associated with neurodegeneration and worse cognition in older adults over a 7-year period despite high levels of physical activity. *Alzheimer's & Dementia*, *21*(5), e70157.

Gong, J., Harris, K., Peters, S. A., & Woodward, M. (2021). Sex differences in the association between major cardiovascular risk factors in midlife and dementia: a cohort study using data from the UK Biobank. *BMC medicine*, *19*(1), 110.

Gong, X., Lin, C., Cheng, J., Su, J., Zhao, H., Liu, T., Zhao, P. (2015). Generation of Multicellular Tumor Spheroids with Microwell-Based Agarose Scaffolds for Drug Testing. *PLoS One, 10*(6), e0130348.

Gultekin, S. K., Albayrak, I. G., Diler, Y., Yalcin, A. D., & Arslan, B. A. (2024). Gene expression analysis in plasma of patients with Alzheimer's disease. *Neuroscience Research Notes*, *7*(1), 302-1

Hansen, D. V., Hanson, J. E., & Sheng, M. (2018). Microglia in Alzheimer's disease. *Journal of Cell Biology*, *217*(2), 459-472.

Hayden, M. R. (2019). Type 2 diabetes mellitus increases the risk of late-onset Alzheimer's disease: ultrastructural remodeling of the neurovascular unit and diabetic gliopathy. *Brain sciences*, *9*(10), 262.

He, G. L., Luo, Z., Yang, J., Shen, T. T., Chen, Y., & Yang, X. S. (2016). Curcumin ameliorates the reduction effect of PGE2 on fibrillar β-amyloid peptide (1-42)-induced microglial phagocytosis through the inhibition of EP2-PKA signaling in N9 microglial cells. *PLoS One*, *11*(1), e0147721.

Heneka, M. T., Carson, M. J., El Khoury, J., Landreth, G. E., Brosseron, F., Feinstein, D. L., ... & Kummer, M. P. (2015). Neuroinflammation in Alzheimer's disease. *The Lancet Neurology*, *14*(4), 388-405.

Heneka, M. T., Van der Flier, W. M., Jessen, F., Hoozemanns, J., Thal, D. R., Boche, D., ... & Riechers, S. P. (2024). Neuroinflammation in Alzheimer disease. *Nature Reviews Immunology*, 1-32.

Hickman, S. E., Allison, E. K., & El Khoury, J. (2008). Microglial dysfunction and defective β-amyloid clearance pathways in aging Alzheimer's disease mice. *Journal of Neuroscience*, *28*(33), 8354-8360.

Huh, D., Hamilton, G. A., & Ingber, D. E. (2011). From 3D cell culture to organs-on-chips. *Trends in cell biology*, *21*(12), 745-754.

Humpel, C. (2015). Organotypic brain slice cultures: A review. *Neuroscience*, *305*, 86-98.

Huskin, G., Chen, J., Davis, T., & Jun, H. W. (2023). Tissue-engineered 3D in vitro disease models for high-throughput drug screening. *Tissue Engineering and Regenerative Medicine*, *20*(4), 523-538.

Honda, K., Casadesus, G., Petersen, R. B., Perry, G., & Smith, M. A. (2004). Oxidative stress and redox-active iron in Alzheimer's disease. *Annals of the New York Academy of Sciences*, *1012*(1), 179-182.

Hong, J., Yoon, D., Nam, Y., Seo, D., Kim, J. H., Kim, M. S., ... & Kim, S. R. (2020). Lipopolysaccharide administration for a mouse model of cerebellar ataxia with neuroinflammation. *Scientific Reports*, *10*(1), 13337.

Innala, M., Riebe, I., Kuzmenko, V., Sundberg, J., Gatenholm, P., Hanse, E., & Johannesson, S. (2014). 3D Culturing and differentiation of SH-SY5Y neuroblastoma cells on bacterial nanocellulose scaffolds. *Artificial cells, nanomedicine, and biotechnology*, *42*(5), 302-308.

Ismail, R., Parbo, P., Madsen, L. S., Hansen, A. K., Hansen, K. V., Schaldemose, J. L., ... & Brooks, D. J. (2020). The relationships between neuroinflammation, beta-amyloid and tau deposition in Alzheimer's disease: a longitudinal PET study. *Journal of neuroinflammation*, *17*(1), 151.

Ivshina, M. P., van't Spijker, H. M., Jung, S., Ponny, S. R., Schafer, D. P., & Richter, J. D. (2022). CPEB1 regulates the inflammatory immune response, phagocytosis, and alternative polyadenylation in microglia. *Glia*, *70*(10), 1850-1863

Jack Jr, C. R., Bennett, D. A., Blennow, K., Carrillo, M. C., Dunn, B., Haeberlein, S. B., ... & Silverberg, N. (2018). NIA-AA research framework: toward a biological definition of Alzheimer's disease. *Alzheimer's & dementia*, *14*(4), 535-562.

Jammalamadaka, U., & Tappa, K. (2018). Recent advances in biomaterials for 3D printing and tissue engineering. *Journal of functional biomaterials*, *9*(1), 22.

Jang, J. H., Lee, S. H., Jung, K., Yoo, H., & Park, G. (2020). Inhibitory effects of myricetin on lipopolysaccharide-induced neuroinflammation. *Brain sciences*, *10*(1), 32.

Janjić, K., Agis, H., Moritz, A., Rausch-Fan, X., & Andrukhov, O. (2022). Effects of collagen membranes and bone substitute differ in periodontal ligament cell microtissues and monolayers. *Journal of Periodontology*, *93*(5), 697-708.

Jin, N., Qian, W., Yin, X., Zhang, L., Iqbal, K., Grundke-Iqbal, I., ... & Liu, F. (2013). CREB regulates the expression of neuronal glucose transporter 3: a possible mechanism related to impaired brain glucose uptake in Alzheimer's disease. *Nucleic acids research*, *41*(5), 3240-3256.

Jin, W., Kam, M. K., Lee, S. W., Park, Y. H., Lee, H. J., & Lee, D. S. (2022). Peroxiredoxin 2 ameliorates AβO-mediated autophagy by inhibiting ROS via the ROS–NRF2–p62 pathway in N2a-APP swedish cells. *Antioxidants*, *11*(10), 1889.

Jung, H., Lee, D., You, H., Lee, M., Kim, H., Cheong, E., & Um, J. W. (2023). LPS induces microglial activation and GABAergic synaptic deficits in the hippocampus accompanied by prolonged cognitive impairment. *Scientific reports*, *13*(1), 6547.

Kapałczyńska, M., Kolenda, T., Przybyła, W., Zajączkowska, M., Teresiak, A., Filas, V., Ibbs, M., Bliźniak, R., Łuczewski, Ł., Lamperska, K. (2018). 2D and 3D cell cultures - a comparison of different types of cancer cell cultures. *Archives of Medical Science, 14(4)*, 910-919.

Kauppinen, T. M., Suh, S. W., Higashi, Y., Berman, A. E., Escartin, C., Won, S. J., ... & Swanson, R. A. (2011). Poly (ADP-ribose) polymerase-1 modulates microglial responses to amyloid β. *Journal of neuroinflammation*, *8*(1), 152.

Kelm, J. M., & Fussenegger, M. (2010). Scaffold-free cell delivery for use in regenerative medicine. *Advanced drug delivery reviews*, *62*(7-8), 753-764.

Ko, K. R., Tam, N. W., Teixeira, A. G., & Frampton, J. P. (2020). SH-SY5Y and LUHMES cells display differential sensitivity to MPP+, tunicamycin, and epoxomicin in 2D and 3D cell culture. *Biotechnology progress*, *36*(2), e2942.

Krishnamurthy, H. K., Jayaraman, V., Krishna, K., Wang, T., Bei, K., Changalath, C., & Rajasekaran, J. J. (2025). An overview of the genes and biomarkers in Alzheimer's disease. *Ageing Research Reviews*, *104*, 102599.

Kulatunga, D. C. M., Ranaraja, U., Kim, E. Y., Kim, R. E., Kim, D. E., Ji, K. B., & Kim, M. K. (2023). Precise Characterization of Differentiated SH-SY5Y Cells Using a Novel APP Splice Variant Dependent Method: for Intended Use in AD Research.

Langhans, S. A. (2018). Three-dimensional in vitro cell culture models in drug discovery and drug repositioning. *Frontiers in pharmacology*, *9*, 6.

Levy-Lahad, E., Wasco, W., Poorkaj, P., Romano, D. M., Oshima, J., Pettingell, W. H., ... & Tanzi, R. E. (1995). Candidate gene for the chromosome 1 familial Alzheimer's disease locus. *Science*, *269*(5226), 973-977.

Li, Y. X., Sibon, O. C. M., & Dijkers, P. F. (2018). Inhibition of NF-κB in astrocytes is sufficient to delay neurodegeneration induced by proteotoxicity in neurons. *Journal of neuroinflammation*, *15*(1), 261.

Lin, H., Dixon, S. G., Hu, W., Hamlett, E. D., Jin, J., Ergul, A., & Wang, G. Y. (2022). p38 MAPK is a major regulator of amyloid beta-induced IL-6 expression in human microglia. *Molecular neurobiology*, *59*(9), 5284-5298.

Linton, M. F., Gish, R., Hubl, S. T., Bütler, E., Esquivel, C., Bry, W. I., ... & Young, S. G. (1991). Phenotypes of apolipoprotein B and apolipoprotein E after liver transplantation. *The Journal of clinical investigation*, *88*(1), 270-281.

Liu, C. C., Kanekiyo, T., Xu, H., & Bu, G. (2013). Apolipoprotein E and Alzheimer disease: risk, mechanisms and therapy. *Nature Reviews Neurology*, *9*(2), 106-118.

Long, H. Z., Zhou, Z. W., Cheng, Y., Luo, H. Y., Li, F. J., Xu, S. G., & Gao, L. C. (2022). The role of microglia in Alzheimer's disease from the perspective of immune inflammation and iron metabolism. *Frontiers in Aging Neuroscience*, *14*, 888989.

Louit, A., Galbraith, T., Berthod, F. (2023). In vitro 3D modeling of neurodegenerative diseases. *Bioengineering*, *10(1),* 93.

M Di Battista, A., M Heinsinger, N., & William Rebeck, G. (2016). Alzheimer's disease genetic risk factor APOE-ε4 also affects normal brain function. *Current Alzheimer Research*, *13*(11), 1200-1207.

Martinsson, I., Quintino, L., Garcia, M. G., Konings, S. C., Torres-Garcia, L., Svanbergson, A., ... & Gouras, G. K. (2022). Aβ/APP-induced hyperexcitability and dysregulation of homeostatic synaptic plasticity in models of Alzheimer's disease. *bioRxiv*, 2022-01.

Mátis, G., Kulcsár, A., Petrilla, J., Talapka, P., & Neogrády, Z. (2017). Porcine hepatocyte–Kupffer cell co-culture as an in vitro model for testing the efficacy of anti-inflammatory substances. *Journal of Animal Physiology and Animal Nutrition*, *101*(2), 201-207.

Mathys, H., Adaikkan, C., Gao, F., Young, J. Z., Manet, E., Hemberg, M., ... & Tsai, L. H. (2017). Temporal tracking of microglia activation in neurodegeneration at single-cell resolution. *Cell reports*, *21*(2), 366-380.

Mensinger, Z. L., Cook, B. L., & Wilson, E. L. (2020). Adsorption of Amyloid Beta Peptide by Metal–Organic Frameworks. *ACS omega*, *5*(51), 32969-32974.

Misun, P. M., Yesildag, B., Forschler, F., Neelakandhan, A., Rousset, N., Biernath, A., ... & Frey, O. (2020). In vitro platform for studying human insulin release dynamics of single pancreatic islet microtissues at high resolution. *Advanced biosystems*, *4*(3), 1900291.

Mórotz, G. M., Glennon, E. B., Greig, J., Lau, D. H., Bhembre, N., Mattedi, F., ... & Miller, C. C. (2019). Kinesin light chain-1 serine-460 phosphorylation is altered in Alzheimer's disease and regulates axonal transport and processing of the amyloid precursor protein. *Acta neuropathologica communications*, *7*(1), 200.

Moss, M. L., Powell, G., Miller, M. A., Edwards, L., Qi, B., Sang, Q. X. A., ... & Bartsch, J. W. (2011). ADAM9 inhibition increases membrane activity of ADAM10 and controls α-secretase processing of amyloid precursor protein. *Journal of Biological Chemistry*, *286*(47), 40443-40451.

Murphy, A. R., Laslett, A., O'Brien, C. M., & Cameron, N. R. (2017). Scaffolds for 3D in vitro culture of neural lineage cells. *Acta Biomaterialia*, *54*, 1-20.

Murphy, M. P., & LeVine III, H. (2010). Alzheimer's disease and the amyloid-β peptide. *Journal of Alzheimer's disease*, *19*(1), 311-323.

Ngamjariyawat, A., Turpaev, K., Vasylovska, S., Kozlova, E. N., & Welsh, N. (2013). Co-culture of neural crest stem cells (NCSC) and insulin producing beta-TC6 cells results in cadherin junctions and protection against cytokine-induced beta-cell death. *PloS one*, *8*(4), e61828.

Niccoli, T., Kerr, F., Snoeren, I., Fabian, D., Aleyakpo, B., Ivanov, D., ... & Partridge, L. (2021). Activating transcription factor 4-dependent lactate dehydrogenase activation as a protective response to amyloid beta toxicity. *Brain communications*, *3*(2), fcab053.

Nordestgaard, L. T., Christoffersen, M., & Frikke-Schmidt, R. (2022). Shared risk factors between dementia and atherosclerotic cardiovascular disease. *International Journal of Molecular Sciences*, *23*(17), 9777.

Ontiveros-Ángel, P., Vega-Torres, J. D., Simon, T. B., Williams, V., Inostroza-Nives, Y., Alvarado-Crespo, N., ... & Figueroa, J. D. (2024). Early-life obesogenic environment integrates immunometabolic and epigenetic signatures governing neuroinflammation. *Brain, Behavior, & Immunity-Health*, *42*, 100879.

Olson, B. J., & Markwell, J. (2007). Assays for determination of protein concentration. *Current protocols in pharmacology*, *38*(1), A-3A.

Pal, R., Bradford, B. M., & Mabbott, N. A. (2022). Innate immune tolerance in microglia does not impact on central nervous system prion disease. *Frontiers in Cellular Neuroscience*, *16*, 918883.

Pankratz, N., Byder, L., Halter, C., Rudolph, A., Shults, C. W., Conneally, P. M., ... & Nichols, W. C. (2006). Presence of an APOE4 allele results in significantly earlier onset of Parkinson's disease and a higher risk with dementia. *Movement disorders: official journal of the Movement Disorder Society*, *21*(1), 45-49.

Park, J. C., Han, J. W., Lee, W., Kim, J., Lee, S. E., Lee, D., ... & Mook-Jung, I. (2024). Microglia gravitate toward amyloid plaques surrounded by externalized phosphatidylserine via TREM2. *Advanced Science*, *11*(34), 2400064.

Park, J., Wetzel, I., Marriott, I., Dréau, D., D'Avanzo, C., Kim, D. Y., ... & Cho, H. (2018). A 3D human triculture system modeling neurodegeneration and neuroinflammation in Alzheimer's disease. *Nature neuroscience*, *21*(7), 941-951.

Perdiguero, E. G., Klapproth, K., Schulz, C., Busch, K., Azzoni, E., Crozet, L., ... & Geissmann, F. Tissue-resident macrophages originate from yolk-sac-derived erythro-myeloid progenitors., 2015, 518.

Phan, D. T., Bender, R. H. F., Andrejecsk, J. W., Sobrino, A., Hachey, S. J., George, S. C., & Hughes, C. C. (2017). Blood–brain barrier-on-a-chip: Microphysiological systems that capture the complexity of the blood–central nervous system interface. *Experimental Biology and Medicine*, *242*(17), 1669-1678.

Pišlar, A., Bolčina, L., & Kos, J. (2021). New insights into the role of cysteine cathepsins in neuroinflammation. *Biomolecules*, *11*(12), 1796.

Price, B. R., Johnson, L. A., & Norris, C. M. (2021). Reactive astrocytes: The nexus of pathological and clinical hallmarks of Alzheimer's disease. *Ageing research reviews*, *68*, 101335.

Priller, C., Bauer, T., Mitteregger, G., Krebs, B., Kretzschmar, H. A., & Herms, J. (2006). Synapse formation and function is modulated by the amyloid precursor protein. *Journal of Neuroscience*, *26*(27), 7212-7221.

Raja, W. K., Mungenast, A. E., Lin, Y. T., Ko, T., Abdurrob, F., Seo, J., & Tsai, L. H. (2016). Self-organizing 3D human neural tissue derived from induced pluripotent stem cells recapitulate Alzheimer's disease phenotypes. *PloS one*, *11*(9), e0161969.

Rajendrakumar, A. L., Arbeev, K. G., Bagley, O., Yashin, A. I., & Ukraintseva, S. (2024). The association between rs6859 in NECTIN2 gene and Alzheimer's disease is partly mediated by pTau. *Frontiers in Aging Neuroscience*, *16*, 1388363.

Ramirez-Bermudez, J. (2012). Alzheimer's disease: critical notes on the history of a medical concept. *Archives of medical research*, *43*(8), 595-599.

Rampersad, S. N. (2012). Multiple applications of Alamar Blue as an indicator of metabolic function and cellular health in cell viability bioassays. *Sensors*, *12*(9), 12347-12360.

Raulin, A. C., Doss, S. V., Trottier, Z. A., Ikezu, T. C., Bu, G., & Liu, C. C. (2022). ApoE in Alzheimer's disease: pathophysiology and therapeutic strategies. *Molecular neurodegeneration*, *17*(1), 72.

Raulin, A. C., Kraft, L., Al-Hilaly, Y. K., Xue, W. F., McGeehan, J. E., Atack, J. R., & Serpell, L. (2019). The molecular basis for apolipoprotein E4 as the major risk factor for late-onset Alzheimer's disease. *Journal of molecular biology, 431(12),* 2248-2265.

Reitz, C., Brayne, C., & Mayeux, R. (2011). Epidemiology of Alzheimer disease. *Nature Reviews Neurology*, *7*(3), 137-152.

Rezai-Rad, M., Bova, J. F., Orooji, M., Pepping, J., Qureshi, A., Del Piero, F., ... & Yao, S. (2015). Evaluation of bone regeneration potential of dental follicle stem cells for treatment of craniofacial defects. *Cytotherapy*, *17*(11), 1572-1581.

Romeo, R., Glotzbach, K., Scheller, A., & Faissner, A. (2021). Deletion of LRP1 from astrocytes modifies neuronal network activity in an in vitro model of the tripartite synapse. *Frontiers in cellular neuroscience*, *14*, 567253.

Roopesh, R. P., Muthusamy, S., Velayudhan, S., Sabareeswaran, A., & Anil Kumar, P. R. (2022). High-throughput production of liver parenchymal microtissues and enrichment of organ-specific functions in gelatin methacrylamide microenvironment. *Biotechnology and Bioengineering*, *119*(3), 1018-1032.

Salih, D. A., Bayram, S., Guelfi, S., Reynolds, R. H., Shoai, M., Ryten, M., ... & Hardy, J. (2019). Genetic variability in response to amyloid beta deposition influences Alzheimer's disease risk. *Brain communications*, *1*(1), fcz022.

Shaltiel, G., Hanan, M., Wolf, Y., Barbash, S., Kovalev, E., Shoham, S., … & Soreq, H. (2012). Hippocampal microrna-132 mediates stress-inducible cognitive deficits through its acetylcholinesterase target. *Brain Structure and Function*, 218(1), 59-72.

Scheuner, D., Eckman, C., Jensen, M., Song, X., Citron, M., Suzuki, N., ... & Younkin, S. (1996). Secreted amyloid β–protein similar to that in the senile plaques of Alzheimer's disease is increased in vivo by the presenilin 1 and 2 and APP mutations linked to familial Alzheimer's disease. *Nature medicine*, *2*(8), 864-870.

Seidel, D., Krinke, D., Jahnke, H. G., Hirche, A., Kloß, D., Mack, T. G., ... & Robitzki, A. (2012). Induced tauopathy in a novel 3D-culture model mediates neurodegenerative processes: a real-time study on biochips. *PLoS One*, *7*(11), e49150.

Sherrington, R., Rogaev, E. I., Liang, Y. A., Rogaeva, E. A., Levesque, G., Ikeda, M., ... & St George-Hyslop, P. H. (1995). Cloning of a gene bearing missense mutations in early-onset familial Alzheimer's disease. *Nature*, *375*(6534), 754-760.

Shiao, Y. H. (2003). A new reverse transcription-polymerase chain reaction method for accurate quantification. *Bmc Biotechnology*, *3*(1), 22.

Sohn, E., Kim, Y. J., Kim, J. H., & Jeong, S. J. (2021). Ficus erecta Thunb. leaves ameliorate cognitive deficit and neuronal damage in a mouse model of amyloid-β-induced Alzheimer's disease. *Frontiers in Pharmacology*, *12*, 607403.

Sivaraman, B., Raji, V., Velmurugan, B. A., & Natarajan, R. (2022). Acetylcholinesterase enzyme inhibitor molecules with therapeutic potential for alzheimer's disease. *CNS & Neurological Disorders-Drug Targets-CNS & Neurological Disorders)*, *21*(5), 427-449.

Sperling, R. A., Aisen, P. S., Beckett, L. A., Bennett, D. A., Craft, S., Fagan, A. M., ... & Phelps, C. H. (2011). Toward defining the preclinical stages of Alzheimer's disease: Recommendations from the National Institute on Aging-Alzheimer's Association workgroups on diagnostic guidelines for Alzheimer's disease. *Alzheimer's & dementia*, *7(3*), 280-292.

Stanca, S., Rossetti, M., & Bongioanni, P. (2023). Astrocytes as neuroimmunocytes in Alzheimer's disease: A biochemical tool in the neuron–glia crosstalk along the pathogenetic pathways. *International Journal of Molecular Sciences*, *24*(18), 13880.

Stanciu, G. D., Luca, A., Rusu, R. N., Bild, V., Beschea Chiriac, S. I., Solcan, C., ... & Ababei, D. C. (2019). Alzheimer's disease pharmacotherapy in relation to cholinergic system involvement. *Biomolecules*, *10*(1), 40.

Stephenson, A. P., Schneider, J. A., Nelson, B. C., Atha, D. H., Jain, A., Soliman, K. F., Renee Reams, R. (2013). Manganese-induced oxidative DNA damage in neuronal SH-SY5Y cells: attenuation of thymine base lesions by glutathione and N-acetylcysteine. *Toxicol Lett, 218*(3), 299-307.

Stoccoro, A., Siciliano, G., Migliore, L., & Coppedè, F. (2017). Decreased methylation of the mitochondrial D-loop region in late-onset Alzheimer's disease. *Journal of Alzheimer's Disease*, *59*(2), 559-564.

Stockburger, C., Gold, V. A., Pallas, T., Kolesova, N., Miano, D., Leuner, K., & Müller, W. E. (2014). A cell model for the initial phase of sporadic Alzheimer's disease. *Journal of Alzheimer's disease*, *42*(2), 395-411.

Sudduth, T. L., Schmitt, F. A., Nelson, P. T., & Wilcock, D. M. (2013). Neuroinflammatory phenotype in early Alzheimer's disease. *Neurobiology of aging*, *34*(4), 1051-1059.

Sun, D., & Jakobs, T. C. (2012). Structural remodeling of astrocytes in the injured CNS. *The Neuroscientist*, *18*(6), 567-588.

Tao, T., Chen, X., Zhou, Y., Zheng, Q., Gao, S., Wang, J., ... & Li, W. (2022). Continued P2X7 activation leads to mitochondrial fission and compromising microglial phagocytosis after subarachnoid haemorrhage. *Journal of Neurochemistry*, *163*(5), 419-437.

Tarasiuk, J., Kapica-Topczewska, K., Szczepański, M., Kochanowicz, J., Mroczko, B., & Kułakowska, A. (2018). Correlations Between Cerebrospinal Fluid Biomarkers Concentration and Severity of Cognitive Impairment in Alzheimer Disease. *Pielęgniarstwo Neurologiczne i Neurochirurgiczne*, *7*(4), 150-154.

Tarricone, G., Carmagnola, I., & Chiono, V. (2022). Tissue-engineered models of the human brain: state-of-the-art analysis and challenges. *Journal of Functional Biomaterials*, *13*(3), 146.

Uddin, M. S., Hasana, S., Hossain, M. F., Islam, M. S., Behl, T., Perveen, A., ... & Ashraf, G. M. (2021). Molecular genetics of early-and late-onset Alzheimer's disease. *Current Gene Therapy*, *21*(1), 43-52.

Vatter, H. A., & Brinton, M. A. (2014). Differential responses of disease-resistant and disease-susceptible primate macrophages and myeloid dendritic cells to simian hemorrhagic fever virus infection. *Journal of virology*, *88*(4), 2095-2106.

Vis, M. A., Ito, K., & Hofmann, S. (2020). Impact of culture medium on cellular interactions in in vitro co-culture systems. *Frontiers in bioengineering and biotechnology*, *8*, 911.

Wainaina, M. N., Chen, Z., & Zhong, C. (2014). Environmental factors in the development and progression of late-onset Alzheimer's disease. *Neuroscience bulletin*, *30*(2), 253-270.

Wang, J., Fourriere, L., & Gleeson, P. A. (2024). Advances in the cell biology of the trafficking and processing of amyloid precursor protein: impact of familial Alzheimer's disease mutations. *Biochemical journal*, *481*(19), 1297-1325.

Wang, P. L., Niidome, T., Akaike, A., Kihara, T., & Sugimoto, H. (2009). Rac1 inhibition negatively regulates transcriptional activity of the amyloid precursor protein gene. *Journal of neuroscience research*, *87*(9), 2105-2114.

Wang, X., Wang, W., Li, L., Perry, G., Lee, H. G., & Zhu, X. (2014). Oxidative stress and mitochondrial dysfunction in Alzheimer's disease. *Biochimica et Biophysica Acta (BBA)-Molecular Basis of Disease*, *1842*(8), 1240-1247.

Weingarten, M. D., Lockwood, A. H., Hwo, S. Y., & Kirschner, M. W. (1975). A protein factor essential for microtubule assembly. *Proceedings of the National Academy of Sciences*, *72*(5), 1858-1862.

Whitehouse, C., Bravington, E., Patir, A., Wei, W., Brownlees, J., He, Y., & Corbett, N. (2025). Investigating connectivity deficits in Alzheimer's disease using a novel 3D bioprinted model designed to quantify neurite outgrowth. *Bioengineering*, *12*(3), 245.

Wightman, D. P., Jansen, I. E., Savage, J. E., Shadrin, A. A., Bahrami, S., Rongve, A., ... & Posthuma, D. (2020). Largest GWAS (N= 1,126,563) of Alzheimer's disease implicates microglia and immune cells. *MedRxiv*, 2020-11.

Wiles, L., Gu, S., Pasqualetti, F., Parvesse, B., Gabrieli, D., Bassett, D. S., & Meaney, D. F. (2017). Autaptic connections shift network excitability and bursting. *Scientific Reports*, *7*(1), 44006.

Yamamoto, S., Hasegawa, K., Yamaguchi, I., Tsutsumi, S., Kardos, J., Goto, Y., ... & Naiki, H. (2004). Low concentrations of sodium dodecyl sulfate induce the extension of β2-microglobulin-related amyloid fibrils at a neutral pH. *Biochemistry*, *43*(34), 11075-11082.

Yan, Y., & Wang, C. (2006). Aβ42 is more rigid than Aβ40 at the C terminus: implications for Aβ aggregation and toxicity. *Journal of molecular biology*, *364*(5), 853-862.

Yin, P., Wang, S., Wei, Y., Wang, X., Zhang, J., Yin, X., ... & Zhu, M. (2020). Maresin1 decreased microglial chemotaxis and ameliorated inflammation induced by amyloid-β42 in neuron-microglia Co-culture models. *Journal of Alzheimer's Disease*, *73*(2), 503-515.

Yokoyama, M., Kobayashi, H., Tatsumi, L., & Tomita, T. (2022). Mouse models of Alzheimer's disease. *Frontiers in Molecular Neuroscience*, *15*, 912995.

Yu, Y., Wang, M., Yu, X., Yan, Y., Yu, B., & Zhang, D. (2022). Targeting Forkhead box O1-aquaporin 5 axis mitigates neuropathic pain in a CCI rat model through inhibiting astrocytic and microglial activation. *Bioengineered*, *13*(4), 8567-8580.

Zhang, F., & Jiang, L. (2015). Neuroinflammation in Alzheimer's disease. *Neuropsychiatric disease and treatment*, 243-256.

Zhang, Y., Li, J., Zhao, Y., Huang, Y., Shi, Z., Wang, H., ... & Gao, Y. (2024). Arresting the bad seed: HDAC3 regulates proliferation of different microglia after ischemic stroke. *Science advances*, *10*(10), eade6900.

Zheng, L., Rubinski, A., Denecke, J., Luan, Y., Smith, R., Strandberg, O., ... & Alzheimer's Disease Neuroimaging Initiative. (2024). Combined connectomics, MAPT gene expression, and amyloid deposition to explain regional tau deposition in Alzheimer disease. *Annals of neurology*, *95*(2), 274-287.

Zhou, Y., Ulland, T. K., & Colonna, M. (2018). TREM2-dependent effects on microglia in Alzheimer's disease. *Frontiers in aging neuroscience*, *10*, 202.

Zhu, H., Yan, H., Tang, N. A., Li, X., Pang, P., Li, H., ... & Lu, Y. (2017). Impairments of spatial memory in an Alzheimer's disease model via degeneration of hippocampal cholinergic synapses. *Nature communications*, *8*(1), 1676.

Zuliani, C. C., da Cunha, J. B., de Souza, V. M., de Andrade, K. C., Moraes, Â. M., & Coimbra, I. B. (2025). Amniotic fluid MSCs for scaffold-free cartilage repair: spheroid fusion and chondrogenic microtissue development. *Future Science OA*, *11*(1), 2476922.